α-Catenin-mediated cadherin clustering couples cadherin and actin dynamics

Chi-Shuo Chen[1], Soonjin Hong[1], Indrajyoti Indra[1], Alina P. Sergeeva[2,3,4,5], Regina B. Troyanovsky[1], Lawrence Shapiro[2,4,6$], Barry Honig[2,3,4,5$], and Sergey M. Troyanovsky[1$]

[1]Department of Dermatology, Northwestern University, The Feinberg School of Medicine, Chicago, IL 60611

[2] Department of Biochemistry and Molecular Biophysics, Columbia University Medical Center, 1150 St. Nicholas Avenue, Russ Berrie Pavilion, New York, NY 10032, USA

[3] Center for Computational Biology and Bioinformatics, Columbia University Medical Center, 1130 St. Nicholas Avenue, New York, NY 10032, USA

[4] Department of Systems Biology, Columbia University, 1130 St. Nicholas Avenue, New York, NY 10032, USA

[5] Howard Hughes Medical Institute

[$] Corresponding authors

Running title: α-catenin/actin binding clusters cadherin

Total number of characters (excluding Mat&Meth, References): 40,000

Key words: Cadherin, alpha-catenin, actin, adherens junctions

Please address all correspondence to:

Dr. Sergey Troyanovsky
Department of Dermatology
Northwestern University
The Feinberg School of Medicine,
303 E. Chicago Ave
Chicago, IL. 60611
Phone: +1 (312) 503-9275
Email: s-troyanovsky@northwestern.edu

Dr. Barry Honig
Department of Biochemistry and Molecular Biophysics
Center for Computational Biology and Bioinformatics
Department of Systems Biology
Howard Hughes Medical Institute
Columbia University Medical Center
1130 St Nicholas Ave, 8th Floor, Rm 815
New York, NY 10032, USA
Phone: +1 (212) 851-4651
E-mail: bh6@columbia.edu

Dr. Lawrence Shapiro
Department of Biochemistry and Molecular Biophysics
Department of Systems Biology
Columbia University Medical Center
1150 St Nicholas Ave, 4th Floor, Rm 402 and 403
New York, NY 10032, USA
Phone: +1 (212) 851-5381
E-mail: lss8@columbia.edu

Abstract

The function of the actin-binding domain of α-catenin, αABD, including its possible role in the direct anchorage of the cadherin-catenin complex to the actin cytoskeleton, has remained uncertain. We identified two point mutations on the αABD surface that interfere with αABD binding to actin and used them to probe the role of α-catenin/actin interactions in adherens junctions. We found that the junctions directly bound to actin via αABD were more dynamic than the junctions bound to actin indirectly through vinculin and that recombinant αABD interacted with cortical actin, but not with actin bundles. This interaction resulted in the formation of numerous short-lived cortex-bound αABD clusters. Our data suggest that αABD clustering drives the continuous assembly of transient, actin-associated cadherin-catenin clusters whose disassembly is maintained by actin depolymerization. It appears then that such actin-dependent αABD clustering is a unique molecular mechanism mediating both integrity and reassembly of the cell-cell adhesive interface formed through weak *cis* and *trans* intercadherin interactions.

Introduction

Classical cadherins are the principal transmembrane receptors of the polymorphic cell-cell adhesive structures generally known as adherens junctions (AJs). AJs establish tight but highly dynamic contacts between cells in virtually all multicellular tissues. One of the key unanswered questions is whether and how intracellular proteins regulate extracellular cadherin adhesive activity. While it has been proposed that such inside-out cadherin signaling is based on cadherin oligomerization by the cytoskeleton (Yap et al., 1997; Adams and Nelson, 1998; Kusumi et al., 1999; Gumbiner, 2005), no direct evidence that such a mechanism controls a cell adhesion in vivo has yet been demonstrated.

In recent years, significant progress has been made in understanding the extracellular cell-cell adhesive interface of AJs which is organized by *trans*- and *cis*-inter-cadherin interactions (Wu et al., 2010; Brasch et al., 2012; Troyanovsky, 2012). Together these two interactions produce an ordered adhesive structure that interconnects adjacent cells (Harrison et al., 2011). However these structures, assembled exclusively through cadherin ectodomains, are quite unstable with respect to their lifetimes, morphologies, and mobility of their components. The stability of such ectodomain-based junctions is significantly increased upon their anchorage to the actin cytoskeleton (Hong et al., 2013). Furthermore, cadherin molecules defective for *cis*-interactions, and therefore, unable to form clusters via their extracellular regions, gain the ability to do so if they interact with actin through a covalently attached actin-binding domain (Hong et al., 2013). These observations suggest that actin filaments can collaborate with extracellular interactions in the formation of AJs. This prompted us to study actin-based mechanisms relevant to cadherin clustering.

Intracellular components of AJs recruit dozens of actin-binding proteins that could in principle participate in cadherin-actin interactions (Kobielak and Fuchs, 2004; Green at al., 2010; Niessen et al., 2011; Ivanov and Naydenov, 2013). Of these, only α-catenin seems to be indispensable. The N-terminal head domain of this protein interacts with cadherin through β-catenin, its C-terminal actin-binding domain (αABD) binds actin filaments, whereas its middle domains (M1, M2, and M3) are thought to control the vinculin-binding site located in the M1 domain (Gomez et al., 2011; Yonemura, 2011). In addition to vinculin, several other actin-binding proteins including EPLIN, ZO1, afadin, α-actinin,

spectrin, merlin, and ajuba have been shown to interact with α-catenin (reviewed in Kobielak and Fuchs, 2004) providing alternative indirect ways for α-catenin to bind F-actin. At least two of these proteins, EPLIN and ZO1, which directly interact with αABD, might constitute alternative linkers between αABD and actin filaments (Imamura et al., 1999; Abe and Takeichi, 2008).

Whether direct αABD binding to actin or alternative indirect mechanisms couple cadherin to actin in AJs is unclear. In-vitro binding assays clearly show that β-catenin binding to α-catenin reduces the actin-binding potential of α-catenin (Drees et al., 2005; Yamada et al., 2005) presumably by inhibiting direct αABD-actin interactions. This suggests that αABD, in the context of the cadherin-catenin complex, can interact with actin only if its actin-binding activity is de-repressed. On the other hand, there is strong evidence that direct or indirect αABD interaction with actin is an essential step in AJ formation (Pappas and Rimm, 2006; Desai et al., 2013; Thomas et al., 2013) and in initiating a mechanotransduction pathway resulting in the recruitment of vinculin (Yonemura et al., 2010).

In this study, we explore the role of direct αABD-actin interactions on AJ structure and dynamics. To this end, we identified a set of αABD point mutants unable to interact with actin *in vitro*. These point mutants allowed us to show that a direct αABD-actin interaction stabilizes AJs, links them to actin filaments and initiates vinculin recruitment by α-catenin. We also present evidence that AJs connected to actin via αABD, in contrast to those connected to the cytoskeleton through vinculin, are highly dynamic. Exploring the underlying mechanism of these differences in dynamics, we found that αABD binds only to actin filaments located in the cell cortex. This binding, which is transient and cooperative, generates short-lived αABD clusters whose lifetimes are controlled by the turnover of actin filaments. We propose that these transient αABD clusters, formed on cortical actin filaments, facilitate clustering of cadherin molecules and mediate AJ dynamics.

Results

Mutants that disrupt the binding of αABD to actin filaments. αABD consists of a 5-helix bundle (residues 671 – 841) and a C-terminal extension (residues 842 – 906), which has been seen in two conformations (Rangarajan and Izard, 2013). In one, the closed conformation, the side chain of the conserved W859 (Fig. S1) inserts into the bundle and the C-terminal extension forms an interface with the bundle. In the open conformation the extension is largely unstructured (Fig. 1a). It is not known whether either of these is the conformation that binds actin. Previous actin co-sedimentation experiments with αABD identified an 18-amino acid-long stretch (residues 865-883) as an actin-binding region (Pappas and Rimm, 2006). Using two recombinant GST-fusion proteins, GST-α(671-883) which bound actin, and GST-α(671-864) which failed to bind actin, we confirmed the importance of the 865-883 region in F-actin binding (Fig. 1b).

A series of three-amino-acid alanine substitutions was introduced within the C-terminal extension and the resulting mutants were tested for interaction with F-actin. These experiments revealed several triple-alanine mutations that significantly decreased this interaction (Fig. 1c). Four of these mutations were selected for alanine-scanning mutagenesis, which ultimately identified four residues – K842, L852, K866, and L869 – that contribute to αABD-binding to F-actin (Fig. 1c). Of these, K866 and L869 are fully exposed in one of the two crystal structures and unstructured in the other. K842 and L852 are buried to a different extent in each structure and, in both cases, link the C-terminal extension to the 5-helix bundle. The bundle itself is unlikely to be affected by any of these mutations. Consistently, circular dichroism (CD) studies suggest that the presence or absence of the 866-906 C-terminal region does not impact the overall structure of αABD (Pappas and Rimm, 2006). Taken together, the results suggest that the four residues we have identified are critical to actin binding either through direct contacts or through an indirect structural role in the binding region.

To further characterize a subset of these mutants, we performed F-actin co-sedimentation assays with increasing concentrations of αABD and a fixed concentration of F-actin (Fig. 1d). Curve fitting yielded an apparent K_D for the intact protein of about 1 μM (Fig. 1e). This value is close to that previously reported, ~0.5 μM (Pappas and Rimm, 2006). The K842A mutant showed some evidence of saturation only at its highest concentration,

suggesting that its affinity for F-actin is about 30 μM (Fig. 1e). The binding affinities of K866A and the deletion mutant GST-α(671-864) were too low to be measured.

Recently, a point mutation, I997A, was identified in the actin binding domain of vinculin that decreases actin binding but has little effect on vinculin folding (Thievessen et al., 2013; Thompson et al., 2014). Since I997 is conserved between vinculin and α-catenin (Figure S1), we tested the analogous mutant in αABD, I792A. Co-sedimentation assays showed that this mutation also significantly decreased binding of αABD to actin (Fig. 1c). I792 is fairly distant (over 25 Å) from the C-terminal extension; it is buried in an interdomain interface in full-length α-catenin, but is exposed on the surface of αABD in isolation (Fig 1a).

Having developed mutants that interfere with αABD actin binding, we are now able to assess the role of this interaction in living cells. We chose three of the characterized mutations (K842A, K866A, and I792A) for further experiments.

Direct αABD binding to actin filaments drives junction formation. We first studied the cadherin-α-catenin chimera EcΔ-Dn-α(280-906). The E-cadherin portion of this chimera harbors an extensive cytoplasmic deletion that removes all known intracellular protein-binding sites including the site for p120 (Fig. 2a). The absence of the latter site, which had not been removed from the cadherin-catenin chimeras used in previous studies (Nagafuchi et al., 1994; Imamura et al., 1999; Desai et al., 2013), excluded an involvement of p120 in any chimera-associated effects. The deleted region was replaced with the photo-switchable fluorescent protein Dendra2 and the C-terminal part of α-catenin (aa 280-906), which includes αABD and all three α-catenin middle domains (M1-M3). The lack of the head domain of α-catenin (aa 1-279) in this chimera simplified data interpretation since it excluded the possibility that this chimera interacted with endogenous β-catenin or underwent homodimerization.

The EcΔ-Dn-α(280-906) chimera produced well-defined intercellular junctions in cadherin-deficient A431D cells (Fig. 2a), which were very similar in morphology to AJs in wt A431 cells (see Indra et al., 2013). Consistent with previous data (Imamura et al., 1999), we found that these junctions recruited vinculin and were attached to radial actin bundles, which were integrated with a network of actin bundles connected to other junctions or to

focal adhesions (Fig. 2a). However, when the chimera contained either the K866A or I792A mutations, these junctions were completely abolished (Fig. 2b). The K842A mutation, which only partially weakened αABD binding to actin in the in vitro assay (see also experiments with Dn-αABD below), did not significantly change the junction-forming properties of the chimera (Fig. 2b). The correlation between the mutant's abilities to form junctions and their actin-binding affinities suggests that the actin-binding site of αABD is essential for the assembly of the chimera's junctions.

The presence of vinculin in the chimera's junctions made it unclear whether αABD continuously anchors the junctions to actin filaments or whether this interaction is transient and is needed only for vinculin recruitment, which then would play the major actin-anchoring function. To clarify this issue, we mutated five key residues of the chimera's vinculin binding site (ΔVin mutation). The resulting chimera still formed actin-associated junctions, which, however, were completely devoid of vinculin (Fig. 2c). The majority of these junctions were also devoid of ZO-1 and EPLIN (Fig. S2, arrows), thus excluding the possibility that the binding of either of these two proteins participates in indirect interaction of αABD with the cytoskeleton in our ΔVin chimera. Taken together, our data strongly suggest that αABD mediates the direct binding of the EcΔ-Dn-α(280-906) chimera to actin, and that this interaction drives junction formation.

Effect of αABD and vinculin on junction morphology. To explore the role of αABD binding to actin in real AJs, we used α-catenin-deficient MDA-MB-468 (468) cells (Fig. 3-6 and S3). In these cells, E-cadherin forms a complex with β-catenin and p120 that could potentially interact with several actin-binding proteins including vinculin (Hazan et al., 1997; Peng et al., 2010; Ray et al., 2013). Nonetheless, 468 cells cannot form cohesive epithelial sheets (Troyanovsky et al., 2011) or interconnect their numerous E-cadherin lateral clusters with the cytoskeleton (Fig. 3a). These clusters are likely formed by *cis* and trans extracellular interactions (Harrison et al., 2011) and by p120- or β-catenin-dependent intracellular interactions. The majority of these clusters were devoid of vinculin, EPLIN, and ZO1 (Fig. S3). The lack of detectable association between these clusters and actin allowed us to use 468 cells to investigate the role of αABD in AJs.

Expression of Dendra2-tagged α-catenin (Dn-αCat) in 468 cells restored epithelial organization of their cell-cell contacts including the apicolateral belts of tight junctions (TJs) and AJs (Fig. 3b,c and 4). In addition, the Dn-αCat-reconstituted cells produced two other types of AJs (Fig. 3b,c) that are also typical of epithelial cells (Takeichi, 2014). Numerous spot-like junctions, variable in their sizes and shapes, formed on their lateral surfaces. These lateral junctions, in contrast to the apicolateral junctions, were devoid of vinculin and were not attached to the phalloidin-positive actin structures (Fig. 3b). These features are similar to those observed for the lateral cadherin clusters of the parental cells. The third type of junctions, vinculin-containing "basolateral" junctions, was located at the base of the cell-cell contacts. These junctions were symmetrically attached to the actin bundles, which eventually merged with the dense network of stress fibers (Fig. 3b,c).

We first sought to confirm published data that α-catenin lacking the vinculin-binding site is able to form actin-associated AJs (Huveneers et al., 2012; Twiss et al., 2012; Desai et al., 2013). Indeed, 468 cells expressing the ΔVin mutant of α-catenin produced vinculin-deficient junctions, the majority of which were also deficient for ZO1 and EPLIN (Fig. S3). These junctions, still aligned with the robust actin-enriched structures (Fig. 5a-c), exhibited noticeable defects: the apicolateral AJs as well TJs were fragmented (Fig. 4) and the actin filaments associated with the basolateral junctions were not integrated with the network of stress fibers (basal focus plane, Fig. 5a). Thus, while α-catenin binding to vinculin is required for normal organization of the AJs, vinculin-deficient AJs, similar to the vinculin-deficient junctions produced by the EcΔ-Dn-α(280-906)-ΔVin chimera, still interact with actin.

Next we introduced the K866A or I792A point mutations into the α-catenin ΔVin mutant. As expected, the resulting mutants Dn-αCat-ΔVin+K866A (Fig. 5c) or Dn-αCat-ΔVin+I792A (Fig. 4) associated with the endogenous lateral cadherin clusters since their β-catenin-binding region remained intact. Importantly, morphologically these clusters were indistinguishable from the cadherin clusters of the wt 468 cells (compare Figs. 5c with 3a). Also similar to the parental cells, no actin-enriched structures were detected in association with these clusters (Fig. 5c) and no TJs were found between these cells (Fig. 4). Basolateral AJs were also undetectable. Such a dramatic effect of the actin-uncoupled αABD point

mutations on the ability of the α-catenin ΔVin mutant to assemble AJs provides strong evidenced that this protein uses its αABD to directly interact with actin filaments in AJs.

The experiments described above suggest that α-catenin interacts with actin in AJs in two ways: a direct interaction through its αABD or an indirect interaction mediated by vinculin. The α-catenin ΔVin mutant, by contrast, can utilize only its αABD. To reveal specific properties of AJs linked to actin only through vinculin, we constructed the α-catenin deletion mutant, Dn-αCat(1-505) (Figure 6a). Its deletion, (aa 506-906) encompassing αABD and the M3 domain, permanently activates the vinculin-binding site located in the α-catenin M1 region (Yonemura et al., 2010; Thomas et al., 2013). Consequently, the Dn-αCat(1-505) mutant can interact with actin only or predominantly through association with vinculin. Indeed, this mutant produced vinculin-enriched AJs (Fig. 6b). Although these junctions clearly associated with actin, their morphology was abnormal: the apicolateral junctions were mostly fragmented (Fig 4 and 6a, apical focus plane) and the basolateral junctions, despite forming actin-enriched structures, were dislocated from the actin bundles (basal focus plane, Fig. 6a). Thus, each of these actin-associated AJs, apicolateral and basolateral, require both vinculin and αABD to achieve their normal morphology.

αABD and vinculin have opposite effects on junction dynamics. Using a Dendra photoconversion assay, we compared the dynamics of the apicolateral junctions formed in 468 cells by intact α-catenin with those formed by Dn-αCat-ΔVin and Dn-αCat(1-505). The results presented in Figure 6c reveal remarkable differences. The Dn-αCat-ΔVin-based junctions, connected to actin via αABD only, were very dynamic, losing nearly 30% of their photoconverted fluorescence within 3 min. The junctions formed by the wild type α-catenin were slightly more stable. Surprisingly, the Dn-αCat(1-505)-based junctions that were linked to the cytoskeleton through vinculin were extremely stable: their photoconverted fluorescence showed no changes during the same time period. These observations suggest that αABD reduces junction stability whereas addition of vinculin enhances it.(Sergey, I don't think it is correct to say that αABD "reduces junction stability". It is the other way round, αABD increases junction stability as does vinculin, though to a greater extent.

Throughout our paper we claim that cadherin based adhesion is not sufficient/stable enough unless we increase stability of AJs by anchorage of cadherin clusters to actin cytoskeleton. The statement "αABD reduces junction stability" contradicts it. The other question is what we mean by "stability" in this case. Since we don't present any cell studies on adhesion strength or migration, we can only refer to either thermodynamic or kinetic stability of the ABD-actin interface. Thermodynamically, Kd constants for both a-catenin ABD and vinculin ABD binding to actin are the same. So it is only feasible to talk about kinetics as I did: "αABD makes junctions more dynamic, whereas addition of vinculin enhances AJ strength") In addition, it appears that wt AJs are controlled primarily by αABD-mediated dynamics

αABD selectively interacts with cortical actin filaments to produce dense clusters. In order to better understand the role of αABD in AJs, we studied the binding of the Dendra2-tagged αABD (Dn-αABD) to the cytoskeleton in A431 cells. Phalloidin staining showed that this fusion protein decorated cortical actin but not stress fibers or bundles associated with AJs (Fig. 7a, see arrows). This finding was further validated in experiments with Latrunculin A. Its high concentration (4 μM) completely depolymerized the actin cytoskeleton and concomitantly abolished Dn-αABD filamentous organization (Fig. 7b). At a low concentration (0.4 μM), Latrunculin A left intact some of the bundles. Yet these bundles remained completely devoid of Dn-αABD, which co-localized with the residual clumps of the cortical filaments (Fig. 7c). In order to confirm αABD localization along the actin cortex, we selectively removed actin bundles while maintaining filaments by blocking myosin II activity with Blebbistatin. This treatment did not affect αABD distribution (Fig. 7d). In the absence of bundles, it became obvious that cortical filaments were not evenly decorated by Dn-αABD suggesting that some filaments have specific preferences for interactions with αABD.

The K866A or I792A point mutations of αABD completely abolished its association with the cortex (Fig. 7e). Another mutation, K842A, by contrast, had no obvious effects on Dn-αABD localization. The clearest differences between these proteins were revealed by confocal microscopy: while the intact Dn-αABD was exclusively cortical, its K866A or

I792A mutants were cytosolic. The K842A mutant exhibited an intermediate phenotype (Fig. 7f). Interestingly, the inability of αABD to interact with actin bundles was evident even when recombinant αABD was added to the permeabilized cells (Fig. 7g).

To increase spatial resolution, we examined the distribution of Dn-αABD using Single Molecular Localization Microscopy (SMLM). This technique, which is able to locate individual Dendra2 molecules at 30 nm resolution, confirmed that Dn-αABD does not uniformly bind to the cortex filaments (Fig. 8). Instead, Dn-αABD was localized in numerous clusters. The longest axis of the clusters reached 400 nm and the apparent density of molecules in the cluster reached ~$5x10^4$ molecules per μm^2 (Fig. 8), consistent with the results of Hansen et al. (2014) who found that actin filaments can be completely covered by αABD. We also imaged cells expressing the Dn-αABD-I792A mutant or Latrunculin A pretreated-cells expressing Dn-αABD. Uncoupling of αABD from actin using either of these techniques dramatically changed cluster appearance: the size of the clusters increased concomitantly with a significant decrease of their molecular density (Fig. 8). The latter value for the majority of the Dn-αABD-I792A clusters was about $2x10^3/\mu m^2$, a ~25-fold reduction from wild-type values. After latrunculin treatment, the individual clusters were impossible to demarcate.

αABD clusters on cortical actin are short-lived. Dn-αABD and its mutants were photoconverted in a small area and the resulting red fluorescence of the spot was monitored over time. Figure 9a shows that the area of its red fluorescence remained constant in size but rapidly decreased in intensity ($t_{1/2}$ ~ 10 s). By contrast, the photoconverted spot of its K842A mutant rapidly expanded in size. A drop in red fluorescence of the other two mutants (K866A, I792A) was too fast to be accurately measured. These results suggest that wt αABD remains bound to the same location while the three mutants diffuse away at rates related to their binding properties (Fig. 1c). The fast decay of wt αABD fluorescence despite its constant spatial localization is consistent with a high turnover of the actin filaments themselves. This explanation requires that a pool of αABD that dissociates from a filament due actin depolymerization must have a higher probability of diffusing away than of rebinding to a neighboring actin filament.

To verify the role of actin filament turnover in αABD dynamics, we globally blocked active intracellular processes by ATP depletion or specifically arrested actin dynamics by a triple-drug cocktail containing Jasplakinolide, Latrunculin B, and Y27632 (Peng et al., 2011). Both these approaches significantly slowed down dissipation of the red fluorescence in case of the intact protein, but not of its K842A mutant (Fig. 9b).

In a complementary approach, we photoconverted Dn-αABD at one part of the cell and tracked the photoconverted molecules in the non-converted "dark" part of the same cell using high temporal resolution TIRF microscopy. We expected that this imaging technique, known as fluorescent speckle microscopy (FSM, Danuser and Waterman-Storer, 2003), would reveal dynamics of the Dn-αABD clusters. Indeed, the photoconverted Dn-αABD was quickly recruited into the numerous speckles in the dark cell areas (Fig. 9c,d. movie S1). The modal lifespan of the speckle was about 200-400 ms (Fig. 9e), and new speckles were produced at the rate of 0.2 speckles/sec/1 μm^2. The majority of the speckles showed virtually no displacement (Fig. 9f). As expected, Dn-αABD, uncoupled from actin either by the point mutation I792A or by actin depolymerization by Latrunculin A, was unable to form the speckles (Fig. 8, Fig. 9c and movies S2, S3).

It is possible that each speckle originates from the fluorescence of a single Dn-αABD molecule. In this case, speckle dynamics represents a behavior of a single molecule in the cluster. Alternatively, a speckle could be formed as a result of simultaneous incorporation of many photoconverted molecules into the same cluster. In the latter case, speckle dynamics would reflect the dynamics of the αABD clusters. To distinguish between these possibilities, we fixed the cells 1 min after photoconversion and the speckles formed around the photoconverted area were gradually photobleached with a 561 nm laser. Figure 9g shows that the speckle photobleaching kinetics were not stepwise indicating that each speckle fluorescence was generated by numerous molecules, thus favoring the second possibility – that speckle dynamics represent dynamics of the αABD clusters. Taken together, this live-imaging study shows that αABD clusters are continuously assembled and disassembled along the actin cortex with a fast turnover rate.

In the aforementioned experiments we used isolated αABD. To validate that this domain is functional in full-length α-catenin, we expressed Dn-αCat and its mutant Dn-αCat-I792A in cadherin-deficient A431D cells at levels comparable to those of endogenous α-catenin (Fig.

S5a). Both proteins were cytosolic and their photoconverted fluorescence dissipated rapidly (Fig. S5b). These observations suggested that Dn-αCat is a freely diffusing cytosolic protein in cadherin-deficient A431D cells. FSM, however, revealed the Dn-αCat forms numerous speckles (Figs. S5c,d), the mean lifetime of which was ~400 ms shorter than speckle's lifetime of isolated αABD (see the legend for Fig. S5d). Speckle formation was undetectable in cells expressing the Dn-αCat-I792A mutant. The predominant cytosolic localization of Dn-αCat in absence of cadherin and the short lifetime of its actin-bound clusters may be due to differences in cooperativity between the binding of αABD and full length α-catenin to actin filaments (Hansen et al., 2013).

We then studied whether αABD could cluster the cadherin-catenin complex. We constructed a Dendra-tagged tail domain of E-cadherin linked to the plasma membrane through a myristoylation signal (Ms-Dn-EcTail, see Fig. S5), which is known to form a complex with the endogenous β- and α-catenins (Nieman et al., 1999). The Ms-Dn-EcTail was found to be concentrated in the areas enriched with cortical actin (Fig. S5f) and FSM revealed the formation of numerous very sharp speckles. Latrunculin A abolished formation of such speckles, while some irregularities in the distribution of the Ms-Dn-EcTail remained (Fig. S5g). It is possible that these irregularities, which were undetectable in the Latrunculin A-treated Dn-αABD- or Dn-αCat-expressing cells, were caused by some β-catenin-based interactions. Speckle stability was approximately the same as that of free α-catenin (compare S5d and h). To show that speckle formation was driven by αABD, we expressed Ms-Dn-EcTail in cells where α-catenin had been stably depleted by α-catenin-specific shRNA or where α-catenin or its I792A mutant was re-expressed in the α-catenin-depleted cells. In agreement with the role of αABD in E-cadherin tail clustering, α-catenin depleted cells as well as those expressing the I792A mutant exhibited the same pattern of Ms-Dn-EcTail distribution as control Ms-Dn-EcTail-expressing cells after Latrunculin A treatment (Fig. S5g).

Discussion

The cadherin ectodomain alone can form junction-like structures through *trans* and *cis* intercadherin interactions (Harrison et al., 2011; Wu et al., 2010; Hong et al., 2010, 2013). These junctions, which likely resemble initial points of cell-cell attachment, are too dynamic and apparently too weak to maintain stable cell-cell adhesion unless they are reinforced by interactions with the actin cytoskeleton (Hong et al., 2013). As a step towards elucidating the interplay between intracellular, actin-binding, and extracellular, adhesive, processes in AJs, we sought to determine how α-catenin interacts with the actin cytoskeleton.

AJs can interact with the actin cytoskeleton using αABD. While *in vitro* experiments have demonstrated that αABD binds directly to F-actin (Rimm et al., 1995; Pappas and Rimm, 2006; Pokutta et al., 2002), the role of this binding *in vivo* has been unclear. Indeed, αABD can also bind to actin indirectly through the actin-interacting proteins ZO1 and EPLIN (Imamura et al., 1999; Abe and Takeichi, 2008), while α-catenin in a cadherin-catenin complex in solution cannot bind actin (Yamada et al., 2005; Drees et al., 2005). Observations showing that αABD deletion attenuates AJ formation (Ozawa, 1998; Imamura et al., 1999; Yonemura et al., 2010; Twiss et al., 2012; Desai et al., 2013; Thomas et al., 2013; Maiers et al., 2013) could be interpreted to imply that deletion of αABD abolishes the binding of α-catenin with vinculin, EPLIN, or ZO1 by removing possible modes of indirect interactions.

In order to clarify whether the *in vivo* interaction of αABD with actin in AJs is direct, indirect, or both, we exploited two new αABD point mutations, which dramatically decrease αABD actin-binding activity *in vitro*. These mutations were inserted into the chimeric

protein EcΔ-Dn-α(280-906), which forms actin-associated AJ-like structures in A431D cadherin-deficient cells. No such structures were observed when the mutant chimeras were expressed. In contrast, the EcΔ-Dn-α(280-906)-ΔVin chimera, missing only the vinculin-binding site, formed actin-associated junctions. ZO1 and EPLIN were also absent from these junctions. Together, these results strongly suggest that, in living cells, α-catenin can associate with actin through direct binding of αABD. However, these results, obtained using chimeric proteins, do not address the possibility that β-catenin/α-catenin interactions inhibit αABD in wt AJs.

To address this issue, we tested the α-catenin mutants in the context of full-length α-catenin transfected into α-catenin-deficient 468 cells. Consistent with results obtained with other vinculin-uncoupled α-catenin mutants (Huveneers et al., 2012; Twiss et al., 2012; Desai et al., 2013) and with vinculin-depleted cells (Watabe-Uchida et al., 1998; Taguchi et al., 2011), the α-catenin ΔVin mutant formed AJs, which, despite being devoid of vinculin, were still associated with an actin-enriched scaffold. Insertion of point mutations that inhibit αABD binding to actin completely abolished this association as well as AJ formation. Taken together, our results obtained using two cell models, A431D and 468 cells, strongly suggest that αABD directly links the cadherin-catenin complex to actin and that this interaction is sufficient for AJ assembly. This implies that the very weak actin-binding activity of α-catenin in the cadherin-catenin complex detected in solution (Yamada et al., 2005; Drees et al., 2005) is enhanced in a cellular context. Whether this activation is based on force-dependent strengthening of αABD binding to actin (Buckley et al., 2014) and/or on *cis* inter-cadherin interactions that could potentially support αABD-actin binding via a cooperative mechanism remains unclear.

A striking feature of the vinculin-deficient junctions is the very fast turnover of the α-catenin mutant Dn-αCat-ΔVin (Fig. 6c). In this respect these junctions are similar to AJs that incorporate wt α-catenin, which are also highly dynamic (Fig. 6c). In contrast, the α-catenin mutant Dn-αCat(1-505), which assembles junctions through vinculin, are significantly less mobile. These findings suggest that the direct binding of αABD to the cytoskeleton is compatible with continuous reassembly of AJs, a process that has been previously reported (Adams et al., 1998; Yamada et al., 2005; Lambert at al., 2007; Cavey

et al., 2008; De Beco et al,. 2009; Hong et al., 2010; Canel et al., 2010). The fact that indirect, vinculin-based binding of α-catenin to actin is associated with much slower dynamics may suggest that vinculin once it interacts with actin suppresses AJ turnover. It is important to note that our staining for tight junctions (Fig. 4), as well as previous studies of force-dependent stabilization of AJs (Yonemura et al., 2010; Huveneers et al., 2012) or AJ-mediated adhesion strength (Thomas et al., 2013) suggested that neither αABD nor vinculin alone could produce fully functional AJs.

αABD forms transient actin-attached clusters. In order to understand how αABD binding to actin assembles AJs while also playing a role in AJ disassembly, we analyzed this binding in living cells. Our experiments reveal three previously unknown features of αABD-actin interactions. First, αABD binds exclusively to the actin cortex, a network of actin filaments attached to the inner face of the plasma membrane (Heuser and Kirschner, 1980; Svitkina et al., 2003; Morone et al., 2006). This observation suggests that AJs form their own actin bundles but do not interact with preexisting bundles, consistent with previous data showing the rapid reorganization of the actin cytoskeleton upon AJ formation (Adams et al., 1998; Vasioukhin et al., 2000). We speculate that some bundle-associated proteins, such as tropomyosin, might interfere with αABD binding either by masking binding sites along the filaments or by stabilizing a filament structure that is incompatible with αABD binding.

The second feature is that αABD, instead of being randomly bound to the cortex, exhibits a highly non-uniform distribution on actin filaments. This can be seen even with conventional immunofluorescence microscopy (Fig. 7d), while super-resolution SMLM shows the formation of discrete dense αABD clusters consisting of hundreds of molecules (Fig. 8). The formation of such clusters is consistent with *in vitro* experiments showing that αABD-actin binding is a highly cooperative process: actin filaments have a tendency to be either fully decorated by αABD or not decorated at all (Hansen et al., 2013), an observation that we have reproduced (data not shown).

The third feature is that cortical αABD clusters are transient and dissociate in a time on the order of seconds (Fig. 9). Experiments with inhibitors of actin dynamics suggest that, at least in part, such short cluster lifetimes result from actin filament depolymerization. Consistently, a previous study found that the lifetime of individual actin filaments in a cell-

cell contact area is about 10 sec (Yamada et al., 2005) while a more recent study suggested that a subpopulation of cortical filaments might have a lifetime significantly less than 5 sec (Fritzsche et al., 2013).

Complementary roles of αABD and extra-cellular cadherin clusters in AJ assembly and dynamics. Each cell in a multicellular tissue must continuously readjust its AJs according to changes imposed by its own motility and by the motility of adjacent cells. At least in part this AJ plasticity is mediated by the intrinsic flexibility of the AJ extracellular cadherin-mediated adhesive interface. This interface in vertebrate classical cadherins is mediated by a strand-swap *trans* interaction and a *cis* interaction, which together define an ordered structure that is similar for the type I cadherins (Harrison et al., 2011). The *trans* adhesive interface exhibits fast rebinding kinetics due to binding intermediates called "X-dimers" (Harrison et al., 2010; Hong et al., 2011). Structural (Harrison et al., 2011), computational (Wu et al., 2010), cell biological (Hong et al., 2013) and biochemical (Troyanovsky et al., 2006, 2007) studies suggest that the AJ adhesive interface in vertebrates is organized in numerous small adhesive clusters, whose individual instability and fast reassembly maintain both integrity and flexibility of the cell-cell interface.

Interactions between cadherin and the cytoskeleton, however, also appear to be unstable, allowing cadherin molecules to move in and out of AJs, with the lifetime of a cadherin molecule bound in an AJ estimated at less than a minute (de Beco et al., 2009; Hong et al., 2010). Our observation that αABD forms transient actin cortex-bound clusters (Figures 8 and 9) suggests the mechanism of such instability. Furthermore, it shows that both the adhesive interface and the actin-binding interface of AJs are maintained in the form of reassembling clusters. This concordance implies that the two types of clusters are functionally interconnected. Experimental studies on basal-to-apical flow of cadherin clusters also support this suggestion (Kametani and Takeichi, 2006). These workers observed that basal-apical flow was disrupted upon αABD deletion, indicating that movement of cadherin clusters depends on αABD/actin clustering. Interestingly, while speckle fluorescent microscopy showed that αABD is able to cluster full-length α-catenin as well as the myristoylated E-cadherin-tail (Fig. S5), we were unable to detect clustering

of full-length E-cadherin (data not shown). This may be due to slow E-cadherin diffusion and a low concentration of this protein at the ventral membrane.

A plausible hypothesis for the mechanism of cadherin/αABD interplay could be that a build-up of cadherins in cell-cell contact regions due to a diffusion trap mechanism and the subsequent formation of small ordered clusters involving *trans* and *cis* interactions between cadherin ectodomains, nucleates formation of αABD-based clusters inside the cell. The αABD-based clusters could, in turn, reinforce the intercadherin interactions in the ectodomain clusters, thereby enhancing their adhesive function. The resulting cadherin/αABD-based clusters – transient, due to actin depolymerization and highly adhesive, due to anchorage to cortical actin filaments – could provide a partial basis for AJ plasticity. In this way, both the intracellular and extracellular regions of cadherins could collaborate to maximize cadherin concentration at intercellular junctions and to enhance the general stability of the junctions. While additional studies are required to firmly establish this hypothesis, an interplay between these two types of clustering mechanisms would explain the highly dynamic nature of the αABD-only junctions (Fig. 6c), the ATP-dependence of cadherin turnover in AJs (Troyanovsky et al., 2006) and why polymerization of new actin filaments is required for AJ integrity (Vasioukhin et al., 2000; Zhang et al., 2005).

Materials and Methods

Plasmids. The plasmids (all in pRcCMV, Invitrogene, Carlsbad, CA) encoding chimeric protein EcΔ-Dn-α(280-906) presented in Fig. 2 were based on EcΔDn (Hong et al., 2010). The general maps of the EcΔ-Dn-α(280-906) chimera, Dn-α-catenin, Dn-αABD and their mutants (also in pRcCMV) are presented in Figs. 2-5. The α-catenin mutation inactivating its vinculin-binding site was constructed based on the structural studies (Choi et al., 2012; Rangarajan, Izard, 2012). It includes five amino acid substitutions to alanine: R329A, R330A, L347A, L348A, and Y351A. The shRNA-target region of a-catenin (CCTGTTCCATCTCAAATAA) in the plasmids used in a-catenin-silenced A431 cells was modified using PCR-directed mutagenesis. The original plasmid encoding human αE-catenin was published (Troyanovsky et al, 2011). All plasmid inserts were verified by sequencing.

Cell culture and transfection. Transfection and growth of A431D, A431, and 468 cells were done as described (Troyanovsky et al., 2011). After antibiotic selection, the cells were sorted for moderate transgene expression by FACS. Lentiviral knock-down (shRNA) plasmids (V2LHS-262377, Open Biosystems, Waltham, MA) were obtained from Dr. Yemelianov. Before use, the GFP-encoding region of this plasmid was deleted. The infected cells were selected with puromicine (5 μg/ml).

Immunofluorescence microscopy. For immunofluorescence, cells were fixed and permeabilized either with methanol-acetone or, in case of phalloidin staining, with 3% formaldehyde-1% Triton X-100, or, in case of anti-vinculin staining, with BM[PEO]3 (see

Indra et al., 2013 for details). Wide-field images were taken using Eclipse 80i Nikon microscope (Plan Apo 100×/1.40 objective lens) and a digital camera (CoolSNAP EZ; Photometrics, Tucson, AZ). The images were then processed using Nikon's NIS-Elements software. The following antibodies were used: mouse anti-E-cadherin and anti-occludin (Zymed Laboratories, South San Francisco, CA); rabbit anti-Dendra2 (Evrogen, Moscow, Russia); mouse anti-β-catenin and ZO1 (BD Biosciences, San Jose, CA); mouse anti-vinculin and rabbit anti-EPLIN (Sigma, St. Louis, MO); goat anti-α-catenin (Santa Cruz Inc, Dallas, TX); rabbit anti-α-catenin N-terminal domain, EP1993Y (abCAM, Cambridge, MA); guinea pig ant-cingulin (provided by Dr. I Hofmann, DKFZ, Heidelberg, FRG). AlexaFluor555 phalloidin and Latrunculin A were purchased from Invitrogen.

Live-cell imaging and data processing. These experiments were performed essentially as described earlier (Hong et al., 2010 and 2013). In brief, cells were imaged (in L-15 plus 10% FBS) by Eclipse Ti-E microscope (Nikon, Melville, NY) at 37ºC controlled with Nikon's NIS-Elements software. The microscope was equipped with an incubator chamber, a CoolSNAP HQ2 camera (Photometrics), Plan Apo 60x/1.40 and Plan Apo VC 100x/1.40 lenses and halogen and mercury light sources. Time-lapse images were taken in both FITC and mCherry filter sets using halogen light that minimized phototoxicity and photobleaching. To analyze cadherin junctional turnover, we used a junctional Dendra photoconversion assay (Hong et al., 2013) in which the point of interest (ϕ =2.5 μm) was photoconverted by a 100 ms-long exposure to the 402 nm wave-length laser. Time-lapse images were then taken in red channel in a stream mode with 1 sec (in Fig. 7h) or in 20 sec intervals with 1 sec (Fig. 6c) of image acquisition time. In some cases, the cells immediately before photoconversion were cultured for 5 min in ATP depletion media (Hong et al., 2010). All images were saved as Tiff files and processed using ImageJ software (National Institutes of Health). In the Dendra photoconversion assay, the red fluorescent intensity was normalized in such a way that 0 and 1 corresponded to the background and the initial (immediately after activation) values. The background value was obtained from the image taken right before the photoconversion. The time course of the intensity change was produced from 10 sets of independent experiments. Mean values were calculated for each time point.

For single molecule localization microscopy, the cells were cultured on glass bottom dish (P35G-1.5, MatTek) for overnight and then fixed with 3% Paraformadehyde and 0.1% glutaraldehyde for 10 min at room temperature. After washing three times the cells were immersed in the freshly prepared image buffer containing 50mM Tris-HCl (pH 8.0), 10mM NaCl, 10% Glucose, 5mg/ml glucose oxidase, 0.4 μg/ml catalase, and 0.1M MEA. Samples were sealed immediately after adding image buffer. Nikon N-STORM system with DU897 camera (Andor Technology) was used for super resolution image acquisition. 20,000-40,000 images were acquired at 29 ms/frame exposure time via TIRF illumination, using a Plan-Apochromatic TIRF 100x 1.49 objective lens. Dendra-fused proteins were activated with 405nm laser, and acquired with 561 nm laser illumination. The images were rendered using the build-in N-STORM single molecule localization analysis algorithms.

For the spinning disk confocal microscopy and fluorescent speckle microscopy, the Nikon-Ti invert microscope equipped with Nikon TIRF illuminator module and Yokogawa CSU-X1 spinning disk unit was used. The cells were imaged in CO2 stage incubator during all live-cell imaging process. To identify the spatial distribution of Dn-αABD and its mutants, 0.3 um-thick optical sections were taken through whole cell using confocal mode with 488nm illumination. Optical sections were aquired using NIS-Elements software (Nikon.) For fluorescent speckle microscopy, Dn-tagged molecules were photoconverted using 405 nm laser within the area of ~ 2.5 μm in diameter, and the converted molecules were imaged for 40 s in the adjacent non-photoconverted area (20x20 μm^2) using the 561 nm laser illumination (30% of intensity was used to minimize photobleaching). Images were acquired using TIRF microscopy with Plan-Apochromatic TIRF 100x 1.49 objective lens and iXon3 camera (Andor Technology) at 5 Hz frame rate. The spatial and temporal positions of the clusters were analyzed using Imaris 7.3 (Bitplane). Background subtraction and fluorescent speckle selection were performed with Imaris build-in algorithms. Image stacks were recorded for each protein (n>5), and more than 1000 speckles were tracked in each image stack. For the cluster photobleach experiment (Fig. 8f), the cells were fixed with 3% paraformadehyde on microscope stage 1 min after photoconversion. Time series images were acquired under same condition as fluorescent speckle microscopy, but with 60% 561 nm laser intensity to photobleach αABD clusters.

Actin co-sedimentation and αABD-incorporation assays. For recombinant GST-fusion protein production, the indicated α-catenin DNA fragments were subcloned into the bacterial expression vector pGEX-4T-1, which places GST in front of the αABD. The resulting plasmids were transformed into BL21(DE3) cells. Protein purification was performed using GST SpinTrap columns with no deviation from the manufacturer's protocol (GE Healthcare, Pittsburgh, PA). The co-sedimentation assay and determination of binding affinities were done according to the published protocol (Pappas and Rimm, 2006). In brief, the pre-polymerized actin filaments (rabbit skeletal muscle actin was purchased from the Cytoskeleton, Denver, CO) in F-buffer (2 mM Tris, pH 8.0, 50 mM KCl, 2 mM MgCl2, 1 mM ATP, 1 mM EGTA, 1 mM DTT) were incubated with pre-cleared (100,000xg for 30 min) recombinant proteins for 30 min at room temperature. The pre-clearing step completely removed non-specific sedimentation of the recombinant proteins in the absence of actin. The reaction was centrifugated at 100,000xg for 30 min. Equivalent volumes of pellet and supernatant fractions were analyzed by SDS-PAGE and densitometry. To assess binding affinities, three independent experiments each of which included αABD and three its mutants were performed, one of which is shown in Fig. 1e. While binding curves for the mutants varied between the experiments, K842A mutant always exhibited slightly better binding than other mutants.

To test αABD binding with specific actin filament structures (Fig. 7g), subconfluent cultures of A431 cells were first incubated for 3 minutes in permeabilization buffer (140 mM KCl, 10 mM HEPES, pH 7.0, 3 mM EGTA, 4 mM $MgCl_2$, 1% BSA and 0.05% saponin) and then for 5 minutes in the same buffer with 1.2 μg/ml of the recombinant polyhistidine/mCherry tagged αABD. Cells then were briefly washed in the same buffer, fixed, and processed for anti-actin staining.

Acknowledgments

We are grateful to Dr. I Hofmann (German Cancer Research Center, Heidelberg, FRG) and Dr. JK Wahl (University of Nebraska) and Drs C. Gottardy and A. Yemelyanov (Northwestern University) for providing anti-cingulin antibody, A431D cells, and a-cat shRNA lentivirus, correspondingly. Sequencing, Flow Cytometry, and SMLM were

performed at the Northwestern University Genetic, Flow Cytometry, and Advanced Microscopy Centers. The work was supported by grants from the National Institutes of Health: AR44016 and AR057992 (to S.T.) and GM062270 (to L.S.), and a grant from a National Science Foundation: MCB-1412472 (to B.H.).

References

Abe K, Takeichi M. 2008. EPLIN mediates linkage of the cadherin catenin complex to F-actin and stabilizes the circumferential actin belt. Proc Natl Acad Sci U S A. 105:13-19.

Adams CL, Nelson WJ. 1998. Cytomechanics of cadherin-mediated cell-cell adhesion. Curr Opin Cell Biol. 10:572-577.

Adams CL, Chen YT, Smith SJ, Nelson WJ. 1998. Mechanisms of epithelial cell-cell adhesion and cell compaction revealed by high-resolution tracking of E-cadherin-green fluorescent protein. J Cell Biol. 142:1105-1119.

Borghi N, Sorokina M, Shcherbakova OG, Weis WI, Pruitt BL, Nelson WJ, Dunn AR. 2012. E-cadherin is under constitutive actomyosin-generated tension that is increased at cell-cell contacts upon externally applied stretch. Proc Natl Acad Sci U S A. 109:12568-12573

Brasch, J., O.J. Harrison, B. Honig, and L. Shapiro. 2012. Thinking outside the cell: how cadherins drive adhesion. *Trends Cell Biol*. 22:299-310.

Buckley CD, Tan J, Anderson KL, Hanein D, Volkmann N, Weis WI, Nelson WJ, Dunn AR. 2014. Cell adhesion. The minimal cadherin-catenin complex binds to actin filaments under force. Science. Oct 31;346(6209):1254211.

Canel M, Serrels A, Anderson KI, Frame MC, Brunton VG. 2010. Use of photoactivation

and photobleaching to monitor the dynamic regulation of E-cadherin at the plasma membrane. Cell Adh Migr. 4:491-501.

Cavey M, Rauzi M, Lenne PF, Lecuit T. 2008. A two-tiered mechanism for stabilization and immobilization of E-cadherin Nature 453:751-756

Choi HJ, Pokutta S, Cadwell GW, Bobkov AA, Bankston LA, Liddington RC, Weis WI. 2012. αE-catenin is an autoinhibited molecule that coactivates vinculin. Proc Natl Acad Sci U S A. 109:8576-8581.

Danuser G, Waterman-Storer CM. 2003. Quantitative fluorescent speckle microscopy: where it came from and where it is going. J Microsc. 211:191-207.

De Beco, S., C. Gueudry, F. Amblard, and S. Coscoy. 2009. Endocytosis is required for E-cadherin redistribution at mature adherens junctions. *Proc Natl Acad Sci U S A*. 106:7010-7015.

Desai R, Sarpal R, Ishiyama N, Pellikka M, Ikura M, Tepass U. 2013. Monomeric α-catenin links cadherin to the actin cytoskeleton. *Nat Cell Biol.* 15:261-273.

Drees F, Pokutta S, Yamada S, Nelson WJ, Weis WI. 2005. Alpha-catenin is a molecular switch that binds E-cadherin-beta-catenin and regulates actin-filament assembly. Cell. 123:903-15.

Fritzsche M, Lewalle A, Duke T, Kruse K, Charras G. 2013. Analysis of turnover dynamics of the submembranous actin cortex. Mol Biol Cell. 24:757-767

Gomez GA, McLachlan RW, Yap AS. 2011. Productive tension: force-sensing and homeostasis of cell-cell junctions. *Trends Cell Biol*. 21:499-505.

Gumbiner, B.M. 2005. Regulation of cadherin-mediated adhesion in morphogenesis.

Nature Rev. Mol. Cell Biol. 6:622-634.

Green KJ, Getsios S, Troyanovsky S, Godsel LM. 2010. Intercellular junction assembly, dynamics, and homeostasis. Cold Spring Harb Perspect Biol. 2:a000125.

Hansen SD, Kwiatkowski AV, Ouyang CY, Liu H, Pokutta S, Watkins SC, Volkmann N, Hanein D, Weis WI, Mullins RD, Nelson WJ. 2013. αE-catenin actin-binding domain alters actin filament conformation and regulates binding of nucleation and disassembly factors. *Mol Biol Cell*. 24:3710-3720.

Harrison OJ, Bahna F, Katsamba PS, Jin X, Brasch J, Vendome J, Ahlsen G, Carroll KJ, Price SR, Honig B, Shapiro L. 2010. Two-step adhesive binding by classical cadherins. Nat Struct Mol Biol. 17:348-357.

Harrison, O.J., X. Jin, S. Hong, F. Bahna, G. Ahlsen, J. Brasch, Y. Wu, J. Vendome, K. Felsovalyi, C.M. Hampton, R.B. Troyanovsky, A. Ben-Shaul, J. Frank, S.M. Troyanovsky, L. Shapiro, and B. Honig. 2011. The extracellular architecture of adherens junctions revealed by crystal structures of type I cadherins. *Structure*. 19:244-256.

Hazan, R. B., Kang, L., Roe, S., Borgen, P. I. and Rimm, D. L. 1997. Vinculin is associated with the E-cadherin adhesion complex. *J. Biol. Chem.* 272, 32448-32453.

Heuser JE, Kirschner MW. 1980. Filament organization revealed in platinum replicas of freeze-dried cytoskeletons. J Cell Biol. 86:212-234.

Hong, S., R.B. Troyanovsky, and S.M. Troyanovsky. 2010. Spontaneous assembly and active disassembly balance adherens junction homeostasis. *Proc Natl Acad Sci U S A*. 107:3528-3533.

Hong, S., R.B. Troyanovsky, and S.M. Troyanovsky. 2011. Cadherin exits the junction by switching its adhesive bond. *J Cell Biol*. 192:1073-1083.

Hong S, Troyanovsky RB, Troyanovsky SM. 2013. Binding to F-actin guides cadherin cluster assembly, stability, and movement. *J Cell Biol*. 201:131-143.

Huveneers S, Oldenburg J, Spanjaard E, van der Krogt G, Grigoriev I, Akhmanova A, Rehmann H, de Rooij J. 2012. Vinculin associates with endothelial VE-cadherin junctions to control force-dependent remodeling. J Cell Biol. 196:641-652

Imamura, Y., M. Itoh, Y. Maeno, S. Tsukita, and A. Nagafuchi. 1999. Functional domains of alpha-catenin required for the strong state of cadherin-based cell adhesion. *J Cell Biol*. 144:1311-1322.

Indra I, Hong S, Troyanovsky R, Kormos B, Troyanovsky S. 2013. The adherens junction: a mosaic of cadherin and nectin clusters bundled by actin filaments. J Invest Dermatol. 133:2546-2554

Ishiyama N, Tanaka N, Abe K, Yang YJ, Abbas YM, Umitsu M, Nagar B, Bueler SA, Rubinstein JL, Takeichi M, Ikura M. 2013. An autoinhibited structure of α-catenin and its implications for vinculin recruitment to adherens junctions. *J Biol Chem*. 288:15913-15925.

Ivanov AI, Naydenov NG. 2013. Dynamics and regulation of epithelial adherens junctions: recent discoveries and controversies. *Int Rev Cell Mol Biol*. 303:27-99.

Jockusch BM, Isenberg G. 1981. Interaction of alpha-actinin and vinculin with actin: opposite effects on filament network formation. Proc Natl Acad Sci U S A. 78:3005-3009.

Kametani Y, Takeichi M. 2006. Basal-to-Apical cadherin flow at cell junctions. Nat Cell Biol.9:92-98

Klingelhöfer J, Laur OY, Troyanovsky RB, Troyanovsky SM. 2002. Dynamic interplay between adhesive and lateral E-cadherin dimers. Mol Cell Biol. 22:7449-7458.

Kobielak A, Fuchs E. 2004. Alpha-catenin: at the junction of intercellular adhesion and actin dynamics. *Nat Rev Mol Cell Biol*. 5:614-625.

Kusumi A, Suzuki K, Koyasako K. 1999. Mobility and cytoskeletal interactions of cell adhesion receptors. Curr Opin Cell Biol. 11:582-590.

Lambert M, Thoumine O, Brevier J, Choquet D, Riveline D, Mège RM. 2007. Nucleation and growth of cadherin adhesions. Exp Cell Res. Nov 15;313(19):4025-40.

Maiers JL, Peng X, Fanning AS, DeMali KA. 2013. ZO-1 recruitment to α-catenin--a novel mechanism for coupling the assembly of tight junctions to adherens junctions. J Cell Sci. 126:3904-3915.

Mège, R.M., J. Gavard, and M. Lambert. 2006. Regulation of cell-cell junctions by the cytoskeleton. *Curr Opin Cell Biol*. 18:541-548.

Morone N, Fujiwara T, Murase K, Kasai RS, Ike H, Yuasa S, Usukura J, Kusumi A. Three-dimensional reconstruction of the membrane skeleton at the plasma mem- brane interface by electron tomography. J Cell Biol 174: 851– 862, 2006.

Nagafuchi A, Ishihara S, Tsukita S. 1994. The roles of catenins in the cadherin-mediated cell adhesion: functional analysis of E-cadherin-alpha catenin fusion molecules. J Cell Biol. 127:235-245.

Nieman MT, Kim JB, Johnson KR, Wheelock MJ. 1999. Mechanism of extracellular domain-deleted dominant negative cadherins. J Cell Sci. 112:1621-1632.

Niessen, C.M., D. Leckband, and A.S. Yap. 2011. Tissue organization by cadherin adhesion molecules: dynamic molecular and cellular mechanisms of morphogenetic regulation. *Physiol Rev*. 91:691-731.

Ozawa M. 1998. Identification of the region of alpha-catenin that plays an essential role in cadherin-mediated cell adhesion. J Biol Chem. 273:29524-29529.

Pappas, D.J., and D.L. Rimm. 2006. Direct interaction of the C-terminal domain of alpha-catenin and F-actin is necessary for stabilized cell-cell adhesion. *Cell Commun Adhes*. 13:151-170.

Peng X, Cuff LE, Lawton CD, DeMali KA. 2010. Vinculin regulates cell-surface E-cadherin expression by binding to beta-catenin. *J Cell Sci*. 123:567-567.

Peng GE, Wilson SR, Weiner OD.A 2011. A pharmacological cocktail for arresting actin dynamics in living cells. *Mol Biol Cell*. 22:3986-94.

Pokutta, S., F. Drees, Y. Takai, W.J. Nelson, and W.I. Weis. 2002. Biochemical and structural definition of the l-afadin- and actin-binding sites of alpha-catenin. *J Biol Chem*. 277:18868-18874.

Rangarajan ES, Izard T. 2012. The cytoskeletal protein α-catenin unfurls upon binding to vinculin. *J Biol Chem*. 287:18492-18499.

Rangarajan ES, Izard T. 2013. Dimer asymmetry defines α-catenin interactions. *Nat Struct Mol Biol*. 20:188-193.

Ray S, Foote HP, Lechler T. 2013. beta-Catenin protects the epidermis from mechanical stresses. *J Cell Biol*. 202:45-52.

Rimm DL, Koslov ER, Kebriaei P, Cianci CD, Morrow JS. 1995. Alpha 1(E)-catenin is an actin-binding and -bundling protein mediating the attachment of F-actin to the membrane adhesion complex. Proc Natl Acad Sci U S A. 92:8813-8817.

Shewan AM, Maddugoda M, Kraemer A, Stehbens SJ, Verma S, Kovacs EM, Yap AS. 2005. Myosin 2 is a key Rho kinase target necessary for the local concentration of E-cadherin at cell-cell contacts. Mol Biol Cell. 16:4531-4542.

Svitkina TM, Bulanova EA, Chaga OY, Vignjevic DM, Kojima S, Vasiliev JM, Borisy GG. 2003. Mechanism of filopodia initiation by reorganization of a dendritic network. J Cell Biol. 160:409-421.

Takeichi M. 2014. Dynamic contacts: rearranging adherens junctions to drive epithelial remodeling. *Nat Rev Mol Cell Biol.* 6:397-410

Taguchi K, Ishiuchi T, Takeichi M. 2011. Mechanosensitive EPLIN-dependent remodeling of adherens junctions regulates epithelial reshaping. *J Cell Biol*. 194:643-656.

Thievessen I, Thompson PM, Berlemont S, Plevock KM, Plotnikov SV, Zemljic-Harpf A, Ross RS, Davidson MW, Danuser G, Campbell SL, Waterman CM. 2013. Vinculin-actin interaction couples actin retrograde flow to focal adhesions, but is dispensable for focal adhesion growth. *J Cell Biol*. 202:163-177.

Thomas WA, Boscher C, Chu YS, Cuvelier D, Martinez-Rico C, Seddiki R, Heysch J, Ladoux B, Thiery JP, Mege RM, Dufour S. 2013. α-Catenin and vinculin cooperate to promote high E-cadherin-based adhesion strength. *J Biol Chem*. 288:4957-4969.

Thompson PM, Tolbert CE, Shen K, Kota P, Palmer SM, Plevock KM, Orlova A, Galkin VE, Burridge K, Egelman EH, Dokholyan NV, Superfine R, Campbell SL. 2014. Identification of an Actin Binding Surface on Vinculin that Mediates Mechanical Cell and Focal Adhesion Properties. *Structure*. 22:697-706.

Troyanovsky, R.B., E.P. Sokolov, and S.M. Troyanovsky. 2006. Endocytosis of cadherin from intracellular junctions is the driving force for cadherin adhesive dimer disassembly. *Mol Biol Cell*. 17:3484-3493.

Troyanovsky,R.B., O. Laur, and S.M. Troyanovsky. 2007.Stable and unstable cadherin dimers: mechanisms of formation and roles in cell adhesion. *Mol Biol Cell*. 18:4343-4352.

Troyanovsky RB, Klingelhöfer J, Troyanovsky SM. 2011. α-Catenin contributes to the strength of E-cadherin-p120 interactions. Mol Biol Cell. 22:4247-4255

Troyanovsky, S. 2012. Adherens junction assembly. *Subcell Biochem*. 60:89-108.

Truong Quang BA, Mani M, Markova O, Lecuit T, Lenne PF. 2013. Principles of E-cadherin supramolecular organization in vivo. Curr Biol. 23:2197-2207.

Twiss F, Le Duc Q, Van Der Horst S, Tabdili H, Van Der Krogt G, Wang N, Rehmann H, Huveneers S, Leckband DE, De Rooij J. 2012. Vinculin-dependent Cadherin mechanosensing regulates efficient epithelial barrier formation. Biol Open. 1:1128-1140.

Vasioukhin, V., C. Bauer, M. Yin, and E. Fuchs. 2000. Directed actin polymerization is the driving force for epithelial cell-cell adhesion. *Cell*. 100:209-219.

Watabe-Uchida, M., N. Uchida, Y. Imamura, A. Nagafuchi, K. Fujimoto, T. Uemura, S. Vermeulen, F. van Roy, E.D. Adamson, and M. Takeichi. 1998. alpha-Catenin-vinculin interaction functions to organize the apical junctional complex in epithelial cells. *J Cell Biol*. 142:847-57

Wu, Y., X. Jin, O. Harrison, L. Shapiro, B.H. Honig, A. Ben-Shaul. 2010. Cooperativity between trans and cis interactions in cadherin-mediated junction formation. *Proc Natl Acad Sci U S A*. 107:17592-17597

Yamada S, Pokutta S, Drees F, Weis WI, Nelson WJ. 2005. Deconstructing the cadherin-catenin-actin complex. *Cell*. 123:889-901.

Yap AS, Brieher WM, Pruschy M, Gumbiner BM. 1997. Lateral clustering of the adhesive ectodomain: a fundamental determinant of cadherin function. Curr Biol. 7:308-315.

Yonemura S, Wada Y, Watanabe T, Nagafuchi A, Shibata M. 2010. alpha-Catenin as a tension transducer that induces adherens junction development. Nat Cell Biol. 12:533-542.

Yonemura, S. 2011. Cadherin-actin interactions at adherens junctions. *Curr Opin Cell Biol*. 23:515-522.

Zhang, J., M. Betson, J. Erasmus, K. Zeikos, M. Bailly, L.P. Cramer, and V.M. Braga. 2005. Actin at cell-cell junctions is composed of two dynamic and functional populations. *J Cell Sci*. 118:5549-5562.

Figure Legends

Figure 1. Characterization of the actin-uncoupled αABD mutants. (**a**) Structure of αABD in the context of α-catenin and in isolation in both open and closed conformations (PDBID 4IGG, chain A and B, respectively). αABD is colored in orange while the other domains of α-catenin (αH, M1, M2, and M3) are grey. The residues that decrease αABD/actin binding *in vitro* upon mutation to alanine (Fig. 1c) are shown as spheres and colored according to conservation score estimated via the ConSurf algorithm (see legend). The conserved W859 is in stick representation. The structurally resolved parts of the C-terminal extension of αABD are colored in blue. I792 is exposed on the surface of αABD in isolation but is buried in the interface between αABD and M1 of full-length α-catenin (pink star). (**b**) SDS-PAGE showing the results of actin co-sedimentation assays with GST-α(671-883) and its deletion mutant GST-α(671-864), each at 3 μM. Pellet (P) and supernatant (S) fractions are shown. Note that the GST-α(671-883) mutant (one asterisk) co-sedimented with the actin filaments, while its deletion mutant, GST-α(671-864), marked by two asterisks, remains in the supernatant. (**c**) *In vitro* actin-binding assays of αABD mutants. The K842-K883 region of αABD (upper line) was divided into triplets and binding of each triple alanine mutant (blue bars) was plotted as the quantity of mutant protein in the Pellet relative to total protein (Pellet+Supernatant). Based on these data, several point mutations were selected (black columns). For comparison, the binding of control proteins, such as GST, GST-α(671-883), and GST-α(671-864), as well as the point mutant GST-α(671-883)-I792A is also shown. (**d**) Co-sedimentation assays with GST-α(671-883) and its K866A point mutant at constant F-actin concentration (1 μM) while varying the amount of GST-tagged proteins (Lig) from 1.5 to 24 μM (**e**) Actin binding curves of GST-α(671-883), GST-α(671-864), GST-α(671-883)-K866A, GST-α(671-883)-K842A, and GST-α(671-883)-I792A. Binding affinities were approximated only for two recombinant proteins that showed evidence of saturation at higher ligand concentrations: K_d(GST-α(671-883) = 1 μM and K_d(GST-α(671-883)-K842A) ~ 30 μM.

Figure 2. Direct αABD binding to actin drives junction formation. (**a-c**) Immunofluorescence microscopy of cadherin-deficient A431D cells expressing the following chimera molecules: (a) EcΔ-Dn-α(280-906); (b) αABD point mutants of the EcΔ-Dn-α(280-906) chimera (K842A, K866A, or I792A); (c) vinculin-uncoupled EcΔ-Dn-α(280-906)-ΔVin mutant. Schematic representation of the chimeras is given atop of the microscopy images. Each chimera includes extracellular, transmembrane, and a 17aa-long cytoplasmic region of E-cadherin lacking all known cytoplasmic protein binding sites (EcΔ). Dn denotes the fluorescent protein Dendra2. α-(280-906) denotes a region of α-catenin, which includes the M1-M3 domains and the C-terminal actin binding domain (αABD). The mutated domains are in yellow. The dash-line boxed regions are magnified on the right or at the bottom. The cells were stained for Dendra2 to reveal chimera (Dn), as well as co-stained with actin (Dn+Act), vinculin (Dn+Vin), or actin and vinculin together. Expression of EcΔ-Dn-α(280-906)-ΔVin mutant results in formation of actin-enriched junctions devoid of vinculin though actin structures which are co-localized with chimera are no longer organized into bundles. Bars: 10 μm

Figure 3. Polymorphism of AJs in α-catenin-expressing 468 cells. (**a**) Immunofluorescence staining of the parental α-catenin-deficient 468 cells for E-cadherin (Ec) and actin filaments (Act). The boxed regions are magnified on the right. Note that E-cadherin molecules can assemble only into tiny clusters. (**b**) Dn-αCat-expressing 468 cells triple stained for Dendra2 (Dn, green), actin (Act, red), and vinculin (Vin, blue). The arrows and the asterisk point to the basolateral and apicolateral junctions, respectively, which are positive for all three markers. The α-catenin-negative focal contacts are indicated by arrowhead. (**c**) Dn-αCat-expressing 468 cells triple stained for Dendra2 (Dn, green), actin (Act, red), and a TJ protein cingulin (Cin, blue). Apical (left) and basal (right) focus planes are shown. Note that the apicolateral AJs associate with TJs and with a fine actin staining (apical focus plane). The lateral cell membranes are enriched with numerous lateral spot-like junctions, which did not show clear association with actin structures. The base of the lateral membranes formed basolateral AJs associated with the radial actin bundles (basal focus plane). Schematic representation of the Dn-αCat is given on the top of image. Dn

denotes the green fluorescent protein Dendra2. αH denotes the head domain of α-catenin implicated in binding to β-catenin and homodimerization. M1-M3 and αABD denote middle domains and αABD of α-catenin, respectively. Bars, 10 μm.

Figure 4. Comparison of junctions formed by Dn-αCat or its mutants in 468 cells. The cells were double-stained for occludin to reveal TJs (upper row), and for Dendra2 to reveal transgene products (bottom row). The maps of Dn-αCa proteins are shown as in Fig. 3. The mutated domains are in yellow. Dn-αCat can interact with actin both directly through αABD and indirectly through vinculin whereas its Dn-αCat-ΔVin and Dn-αCat(1-505) mutants can only associate with actin specifically through αABD or vinculin, respectively. Both modes of interactions are inactivated in the double mutant Dn-αCat-ΔVin+I792A. Note that cells expressing intact α-catenin were the only ones to produce fully-closed rings of TJs. All the mutants showed comparable levels of expression (Fig. S4a). Bars, 40 μm.

Figure 5. AJs interact with actin filaments through αABD. (a-c) Immunofluorescence microscopy of 468 cells expressing (a-b) the α-catenin mutant, which interacts with actin specifically through αABD, Dn-αCat-ΔVin, or (c) the same mutant with additional K866A point mutation. (a) Cell were double-stained for Dendra2 (Dn) and actin (Act), or (b) Dn and vinculin (Vin). The boxed regions are magnified on the right. (**a**) The apical and basal focus planes are shown. Many apicolateral AJs of these cells were associated with the radial actin bundles. The cells were completely unable to produce basolateral AJs. (**b**) Vinculin is recruited only into the focal contacts. (**c**) 468 cells expressing Dn-αCat-ΔVin-K866A chimera have a phenotype similar to that of the parental cells (Fig. 3a). Bars, 10 μm.

Figure 6. AJs interacting with actin through vinculin produce adynamic junctions. (**a,b**) Immunofluorescence microscopy of 468 cells expressing the α-catenin deletion mutant, Dn-αCat(1-505). Cell were double-stained for (a) Dendra2 (Dn) and actin (Act), or (b) Dn and vinculin (Vin). (**a**) Apicolateral AJs are associated with fine actin structures (apical focus plane). The basolateral junctions were also present but not associated with actin bundles (arrows, basal focus plane). (**b**) Apicolateral and lateral junctions both recruit

vinculin. Bars, 10 μm. (**c**) Dendra photoconversion assay of the apicolateral AJs in 468 cells expressing Dn-αCat, Dn-αCat-ΔVin, or Dn-αCat(1-505). The intensity of the red fluorescence in the photoconverted spots decreases over time. The error bars represent SEs (n=20).

Figure 7. Selective interaction of αABD with the actin cytoskeleton. (**a-d**) Spatial localization of Dn-αABD (Dn, green, stained for Dendra2) and actin filaments (Act): (a) in A431 cells; (b) in A431 cells treated with a high dose of Latrunculin A for 10 min; (c) in A431 cells treated with a low dose of Latrunculin A for 10 min; (d) in A431 cells treated with Blebbistatin for 15 min. The Dn-αABD chimera includes Dendra2 (Dn, green) and the 671-906 region of α-catenin (αABD, red). (**e**) Spatial localization of the Dn-αABD point mutants – K842A, I792A, and K866A – in A431 cells. (**f**) Confocal microscopy of A431 cells expressing Dn-αABD and its point mutants – K842A and K866A in horizontal and vertical confocal sections. (g) Wild type A431 cells were permeabilized with 0.025% saponin for 3 min and then incubated for another 5 min with His-mCherry tagged αABD (αABD) or its inactive I792A version (αABD-I792A) and stained for actin. Note that αABD preferentially decorates the cortex but shows very weak binding to the actin bundles. The I792A mutant shows only non-specific binding. Arrows point to bundles (a and g) and cortical clumps (c). Bars: 10 μm (a-f), 20 μm (g).

Figure 8. Single-molecule localization microscopy (SMLM) of αABD clusters. A431 cells expressing Dn-αABD (αABD), its point mutant Dn-αABD-I792A (I792A), or Dn-αABD following a 10-min treatment with Latrunculin A (LnA). The corresponding heat maps of molecular cluster densities are shown at the bottom with the heat bar given in the right corner.

Figure 9. Dynamic properties of αABD clusters. (**a**) Dendra photoconversion assay of A431 cells expressing Dn-αABD (αABD) or its K842A or K866A point mutants. The images of green (-2) and red (-1) fluorescence were taken two and one sec before photoconversion, respectively. The encircled areas (d=2.5 μm) were converted from green

to red fluorescence at time 0. After photoconversion, the red fluorescence was imaged in a stream mode with image acquisition time of one second. Selected frames taken one, six, or eleven seconds after photoconversion (+1, +6, +11) are shown. (**b**) Red fluorescence intensity over time in the photoconverted spots of A431 cells expressing Dn-αABD or its K842A point mutant. The curves were plotted based on experiments shown in Fig. 8a (repeated 15 times) in unaffected A431 cells (control), in the cells with cytoskeleton stabilized by ATP-depletion (ATP depletion), and in the cells with actin dynamics arrested by a triple-drug cocktail (JYL). Error bars indicate SEs. (**c**) Fluorescent speckle microscopy of A431 cells expressing Dn–αABD or its I792A point mutant. The encircled areas of the cells (d~2.5 μm) were photoconverted to image the adjacent area (yellow box) for 40 sec in a stream mode with 200 ms acquisition time (Movies S1 and S2, correspondingly). Frames taken 20 sec after photoconversion (+20) are shown in the images on the right. (**d**) Spatial localization of αABD speckles plotted based on the movies S1. The color of a given speckle corresponds to the moment of its appearance (the time bar is given at the bottom). (**e**) Lifetime distribution of αABD speckles. (**f**) Displacement of speckles (in nm) during their entire lifetime. (**g**) The photobleaching curves of the individual speckles.

Figure S1. Multiple sequence alignment of orthologous actin binding domains of α-catenin and vinculin.

Figure S2. Junctions made of the EcΔ-Dn-α(280-906)-ΔVin chimera in A431D cells are devoid of the actin-binding proteins ZO1 and EPLIN.

Figure S3. AJs of α-catenin-deficient 468 cells (a) and the same cells expressing Dn-αCat-ΔVin mutant (b).

Figure S4. (a) Western blotting assays using the anti-α-Catenin antibody (EP1993Y) to probe expression levels of Dn-αCat and its mutants. Note that the parental 468 cells do not express endogenous α-catenin. (b) Anti-Dendra Western blot assays of A431 cells probing levels of expression of Dn-αABD and its point alanine mutants – K842A, K866A, and I792A.

Figure S5. Dynamic properties of clusters formed by the full-length α-catenin (upper panel) and myristoylated E-cadherin tail (bottom panel).

Movie S1. Fluorescent speckle microscopy of Dn-αABD clusters in A431 cells. Dn αABD was first photoconverted outside of the imaging area (see Fig. 8c for details) and then the photoconverted molecules were monitored by TIRF microscopy for 40 sec in a

stream mode with 200 ms acquisition time. Note, the photoconverted Dn-αABD produces numerous short-lived clusters.

Movie S2. Fluorescent speckle microscopy of Dn-αABD in Latrunculin A-treated A431 cells. The experiment was performed exactly as described in the legend for Movie S1.

Movie S3. **Fluorescent speckle microscopy of Dn-αABD-I792A mutant in A431 cells** (see Movie S1 for details). Note that the mutant cannot produce clusters.

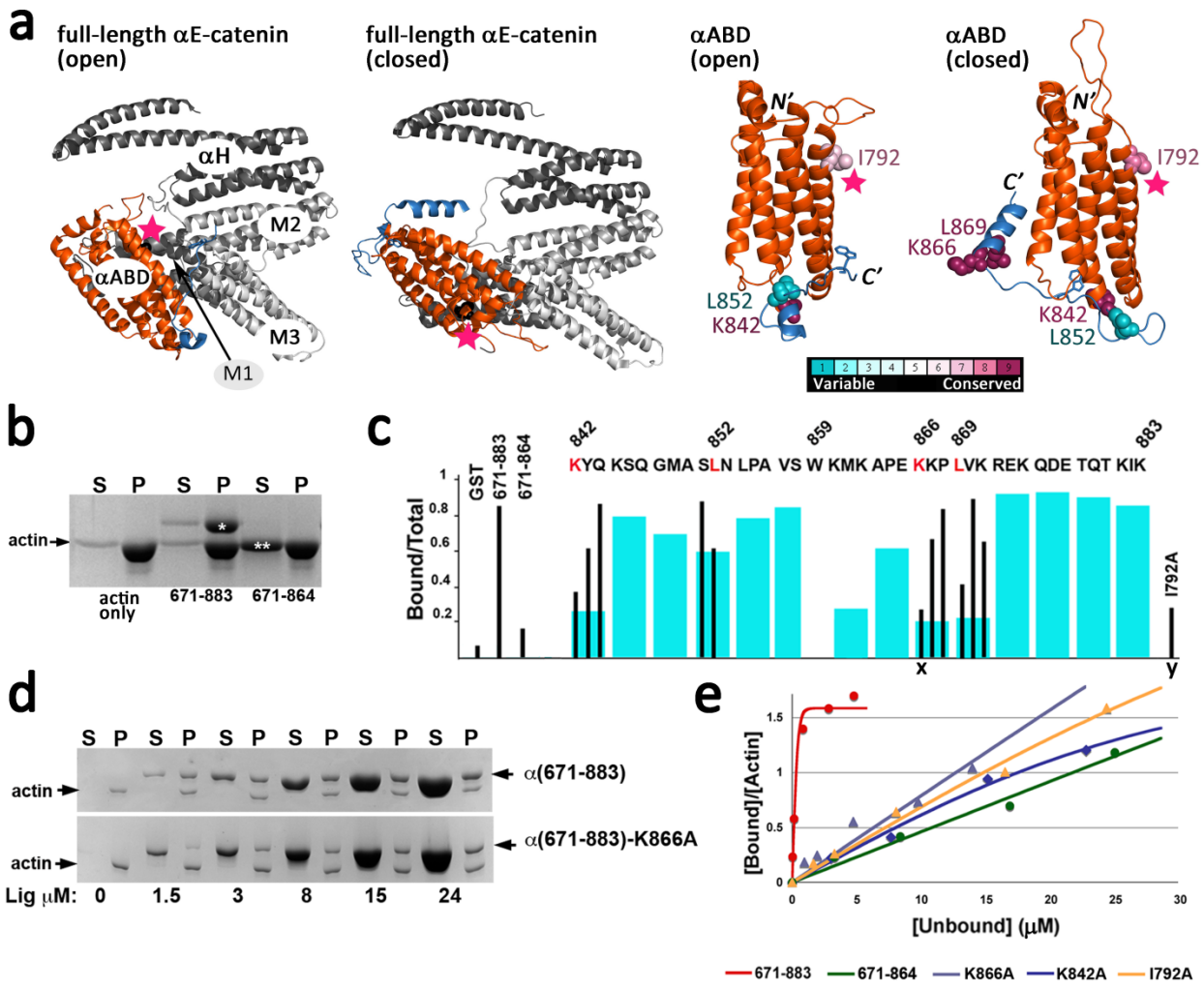

Figure 1 (2-column width)

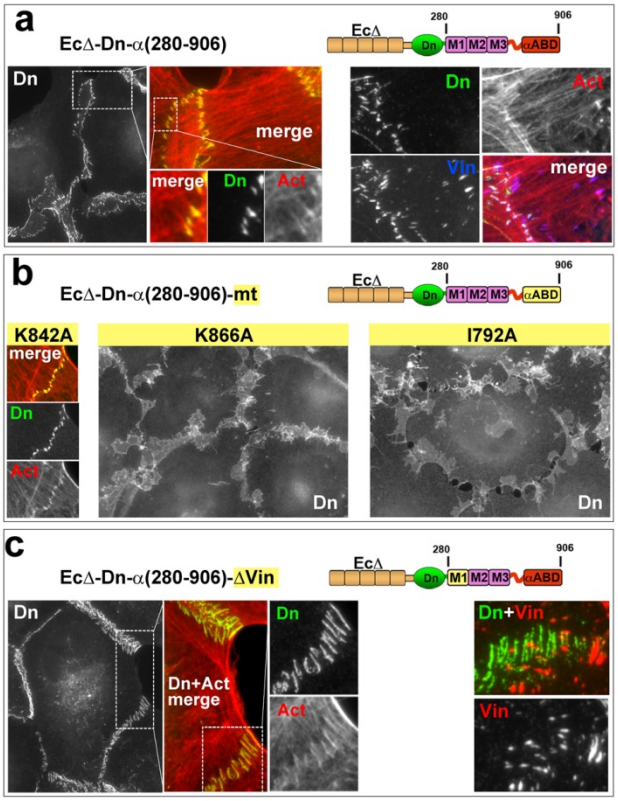

Figure 2 (1-column width)

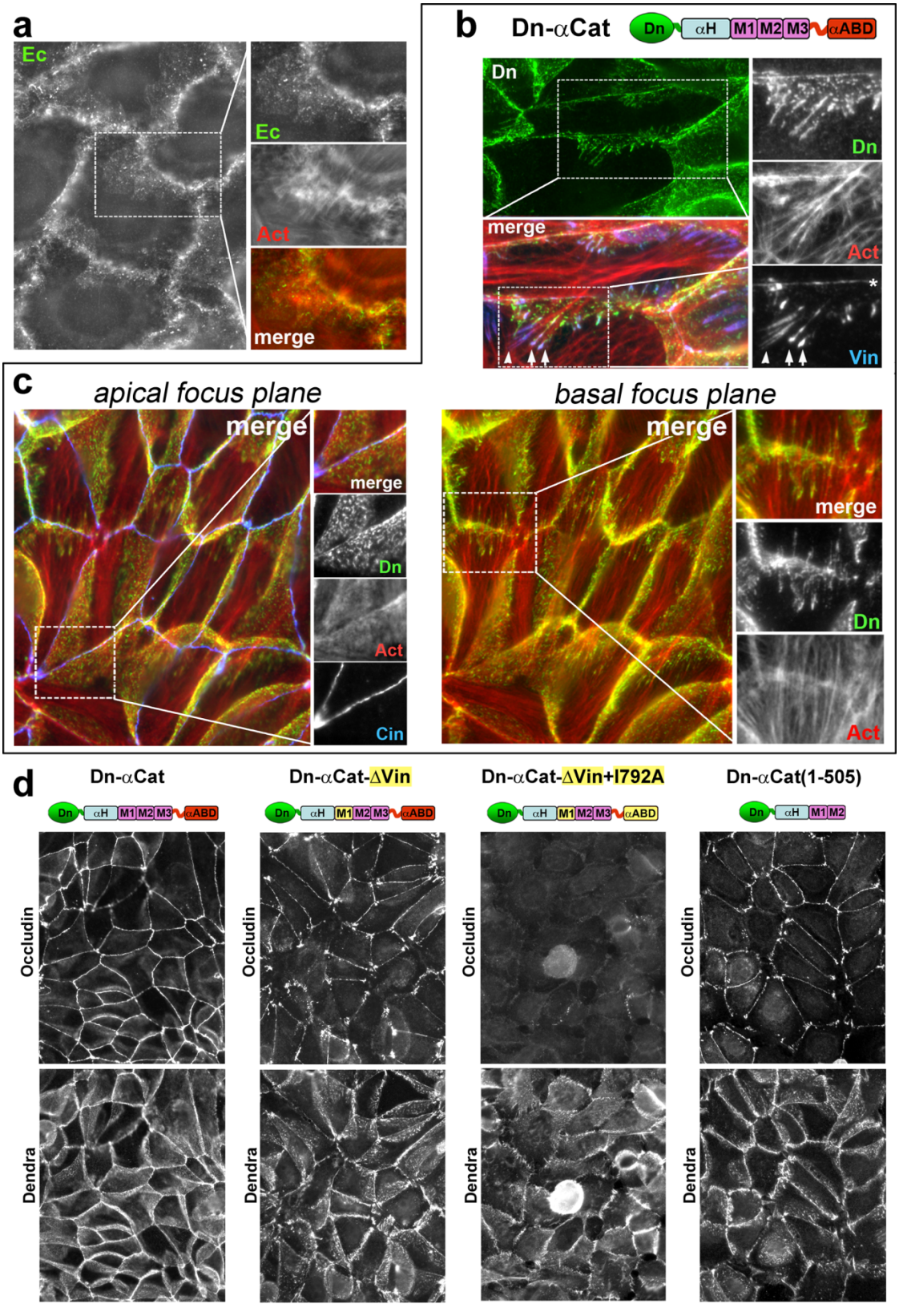

Figure 3+4 (2-column width)

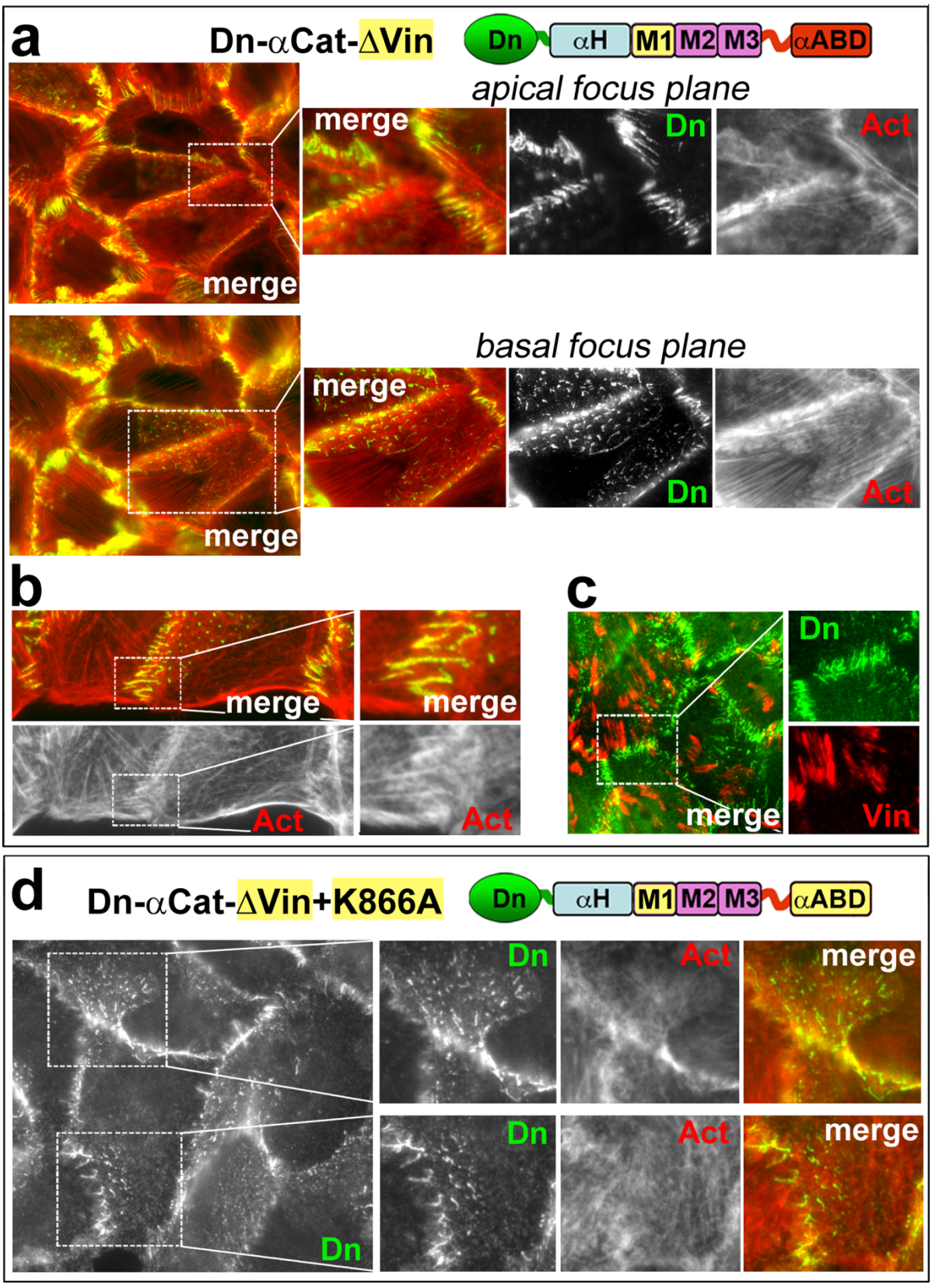

Figure 5 (2-column width)

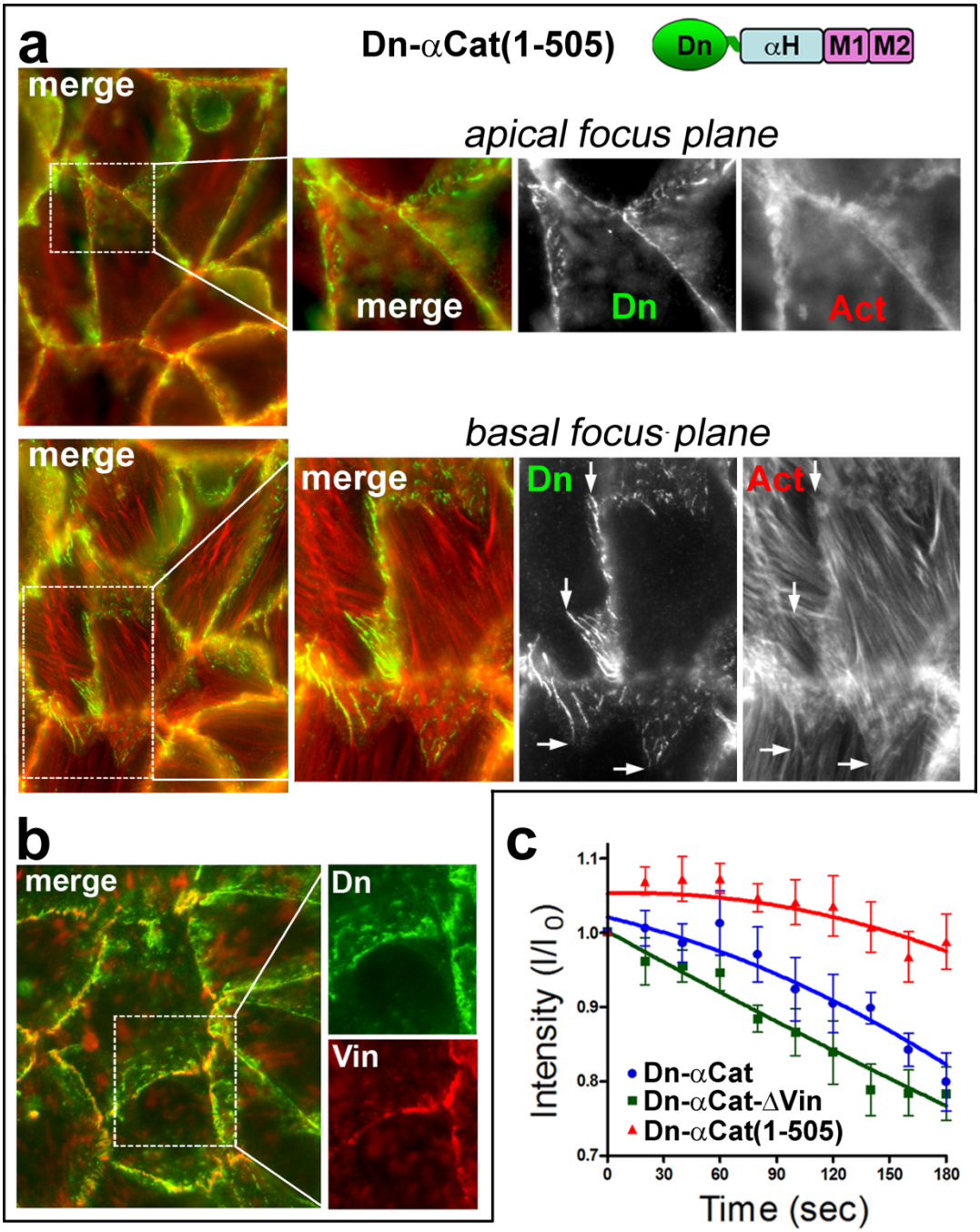

Figure 6 (2-column width)

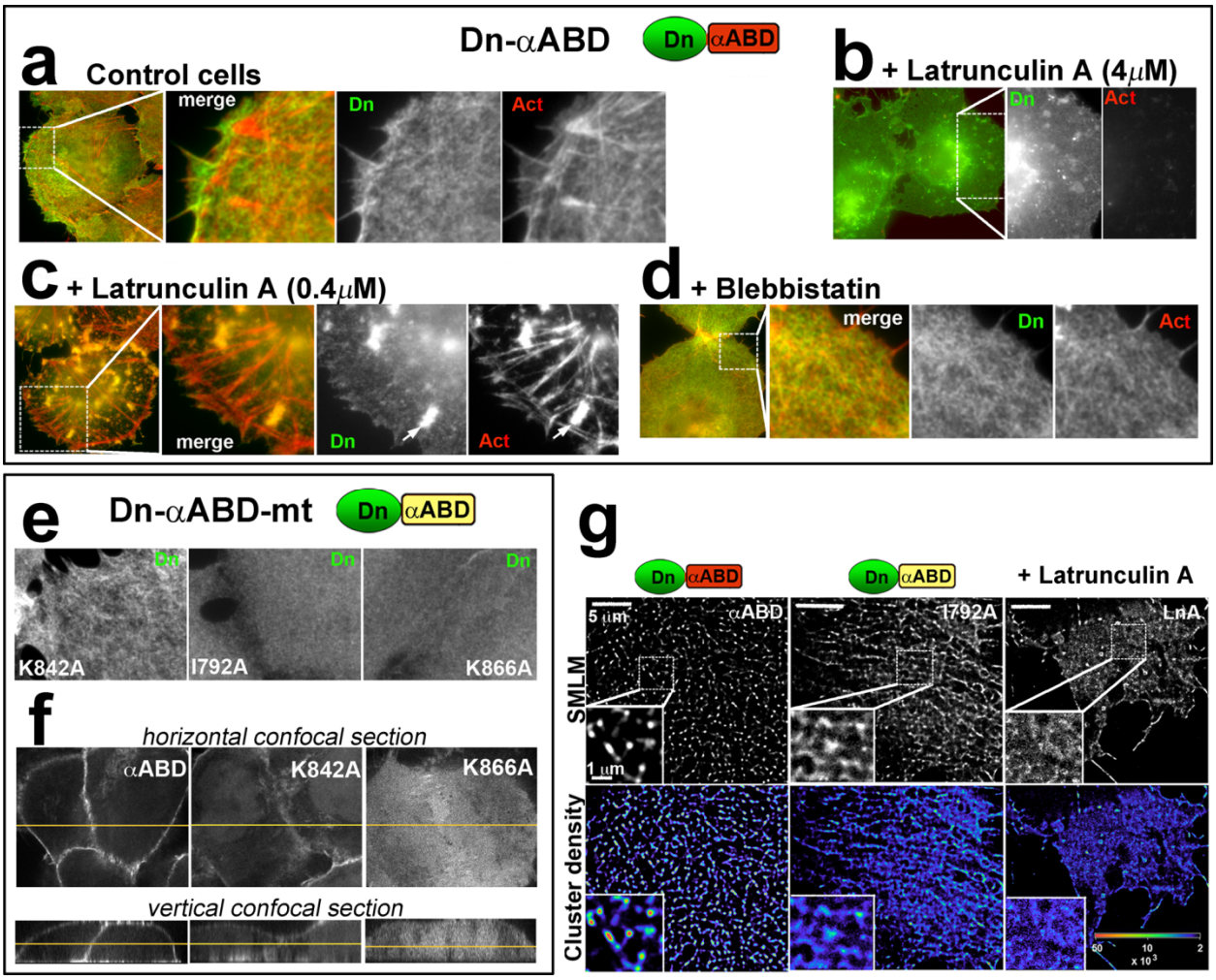

Figure 7 (lacks the final version of 7g whereas this g ended up being the final Figure 8 (2-column width)

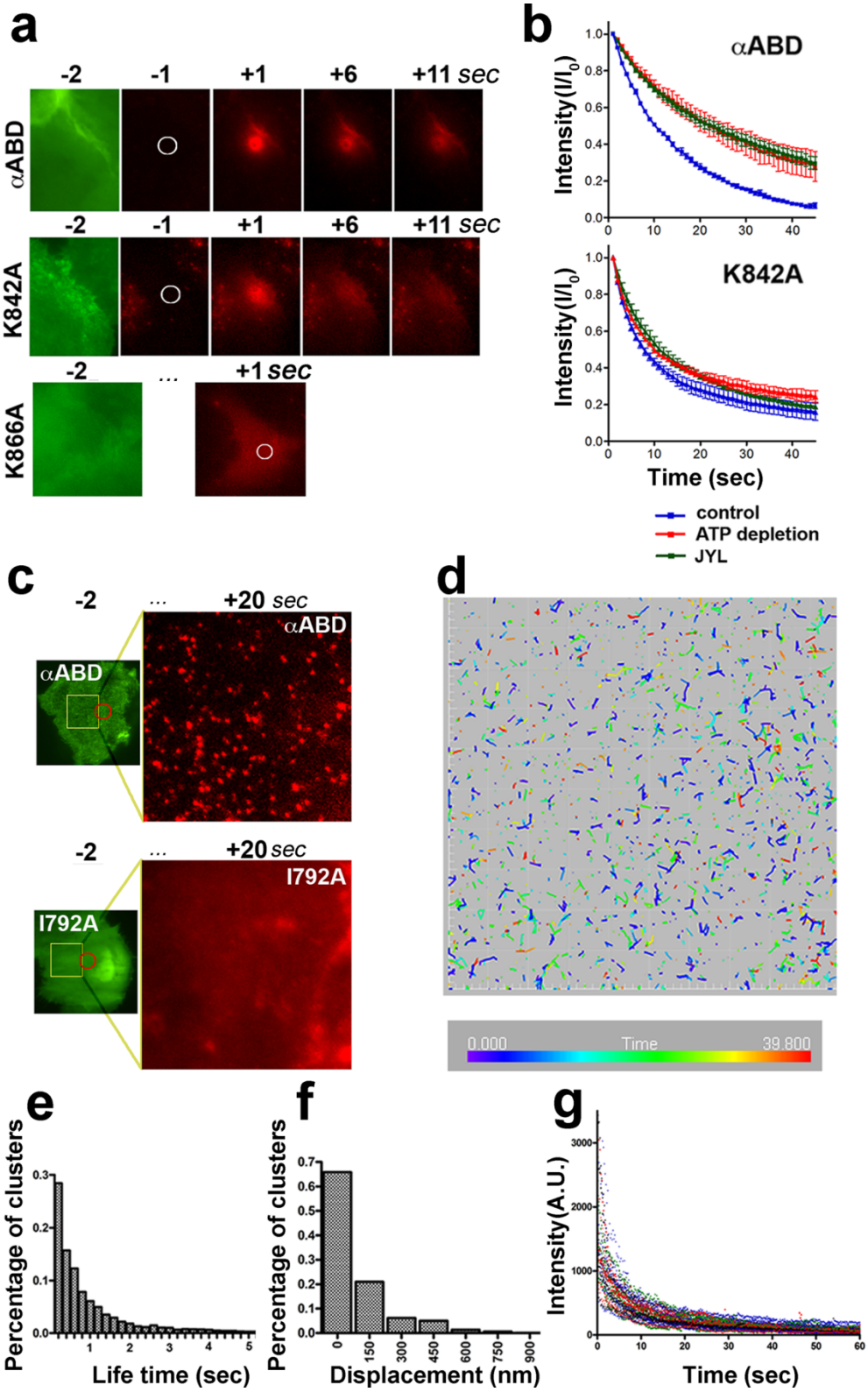

Figure 9 (2-column width)

SUPPLEMENTARY INFORMATION

α-Catenin-mediated cadherin clustering couples cadherin and actin dynamics

Chi-Shuo Chen, Soonjin Hong, Indrajyoti Indra, Alina P. Sergeeva, Regina B. Troyanovsky, Lawrence Shapiro, Barry Honig, and Sergey M. Troyanovsky

Contents:

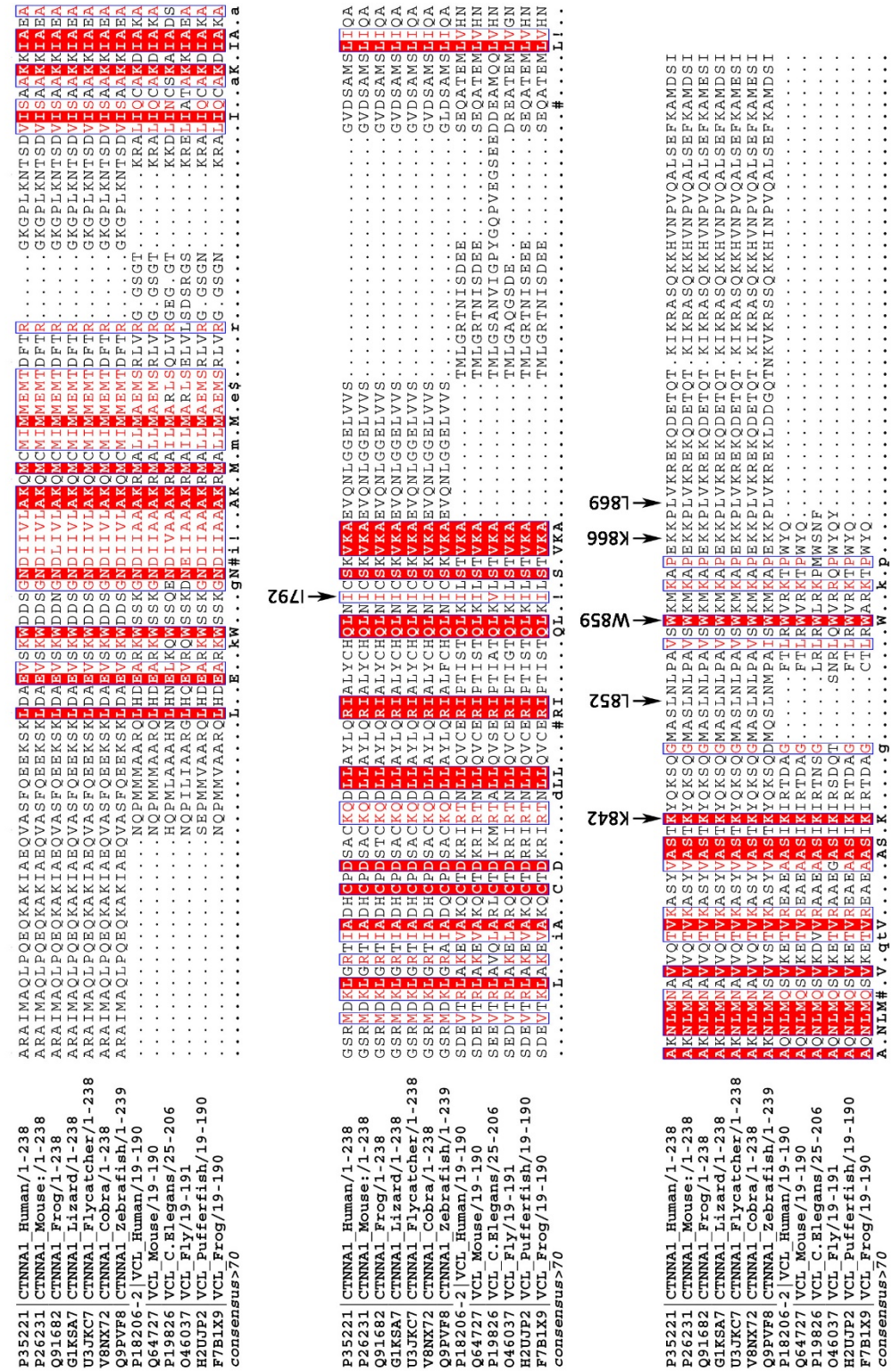

Figure S1. Multiple structure-based sequence alignment of orthologous actin binding domains of α-catenin and vinculin. Point mutants that decreased αABD binding to actin are marked. All the residues are colored using %Equivalent similarity scheme as implemented in ESPript 3.0. Higher percentage of equivalent residues considering their physic-chemical properties corresponds to brighter red color.

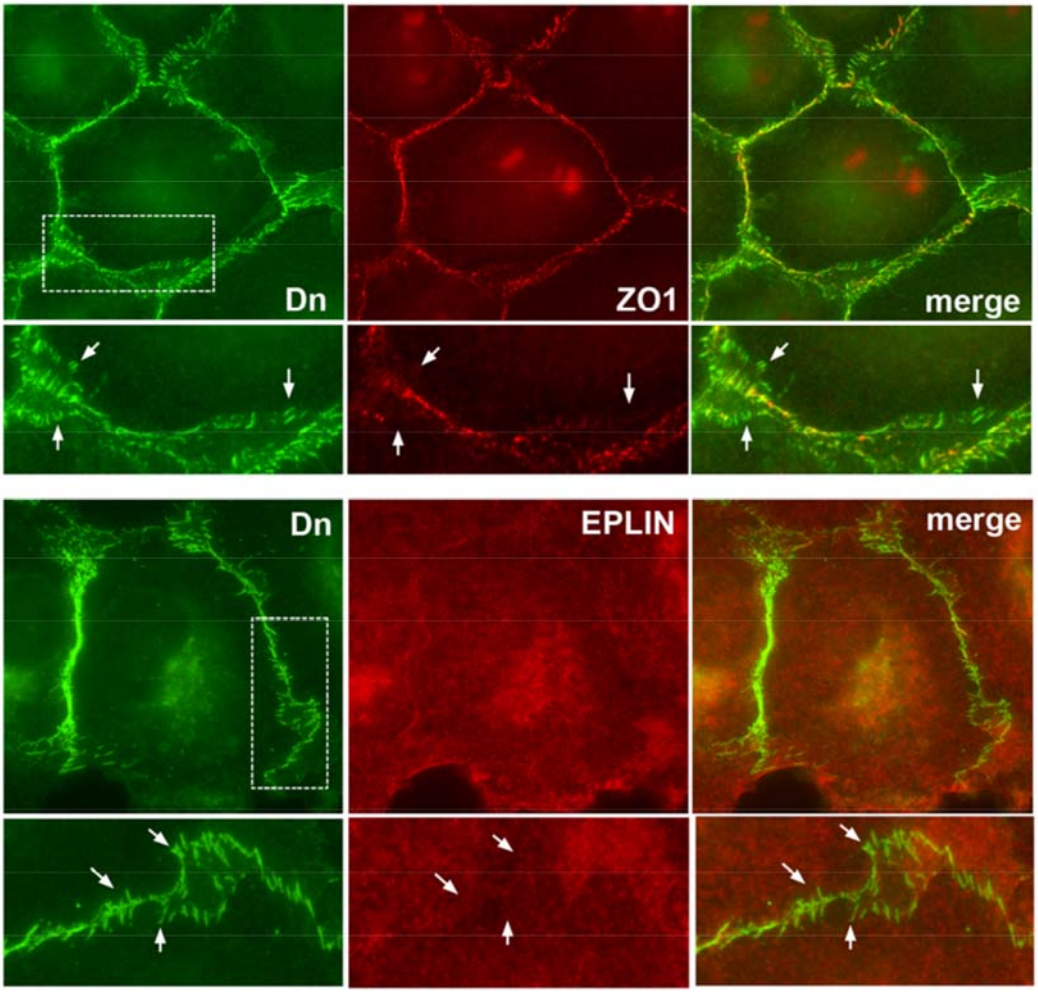

Figure S2. Junctions made of the EcΔ-Dn-α(280-906)-ΔVin chimera in A431D cells are devoid of the actin-binding proteins ZO1 and EPLIN. A431D cells expressing EcΔ-Dn-α(280-906)-ΔVin were double stained for Dendra2/ZO-1 (upper panel) and Dendra2/EPLIN (bottom panel). The selected regions are magnified under the main images. Arrows indicate some of the junctions that completely lack ZO1 or EPLIN signals.

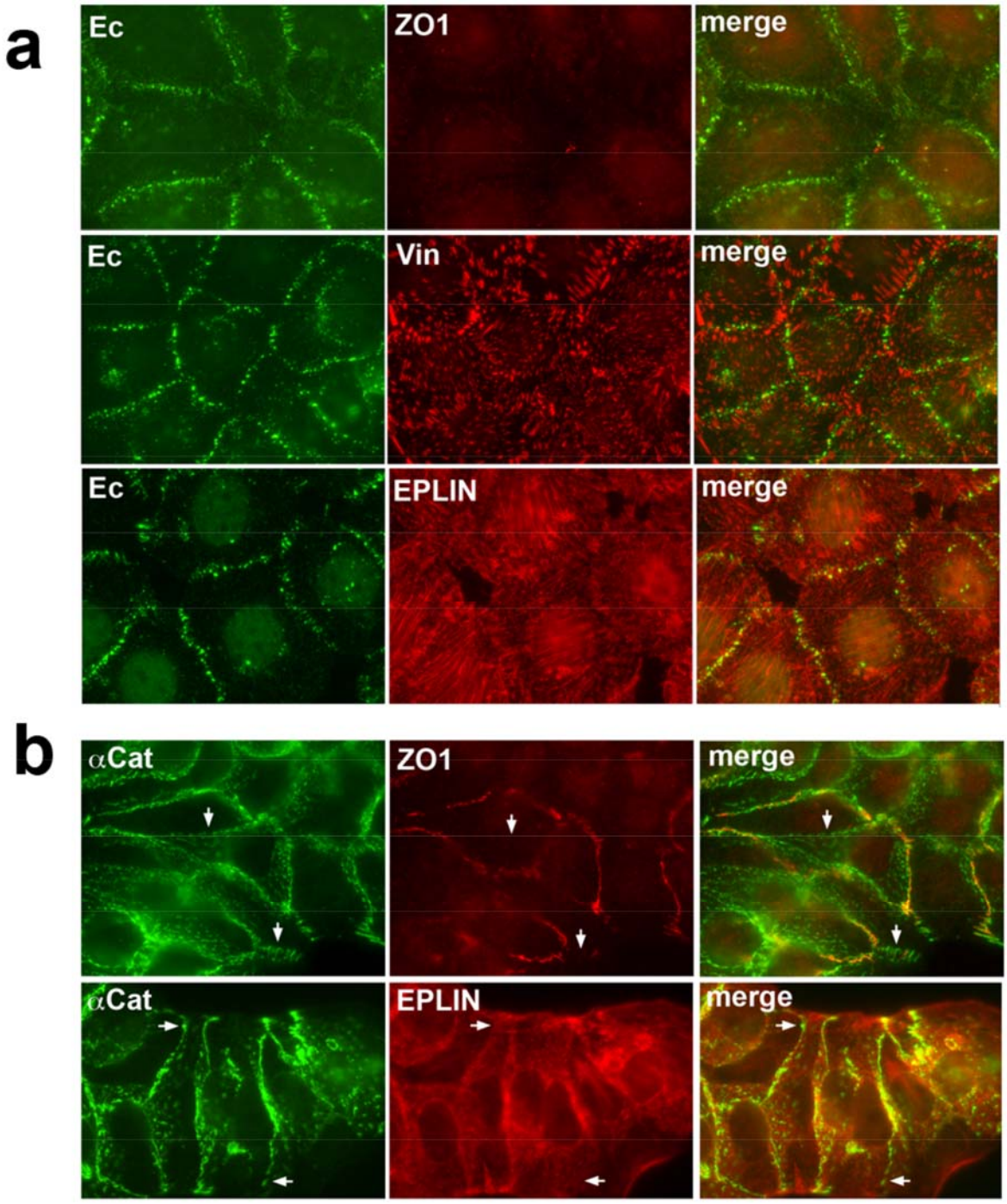

Figure S3. AJs of α-catenin-deficient 468 cells (a) and the same cells expressing Dn-αCat-ΔVin mutant (b). (a) 468 cells were double-stained for E-cadherin (Ec, green) and ZO1 (ZO1), vinculin (Vin), or EPLIN (EPLIN). Note that E-cadherin-positive AJs do not exhibit staining for any of these three actin-binding proteins. (**b**) 468 cells expressing vinculin-uncoupled mutant Dn-αCat-ΔVin were stained for α-catenin (αCat, green) and ZO1 (ZO1) or EPLIN (EPLIN). Some of AJs lacking these two proteins are indicated by arrows.

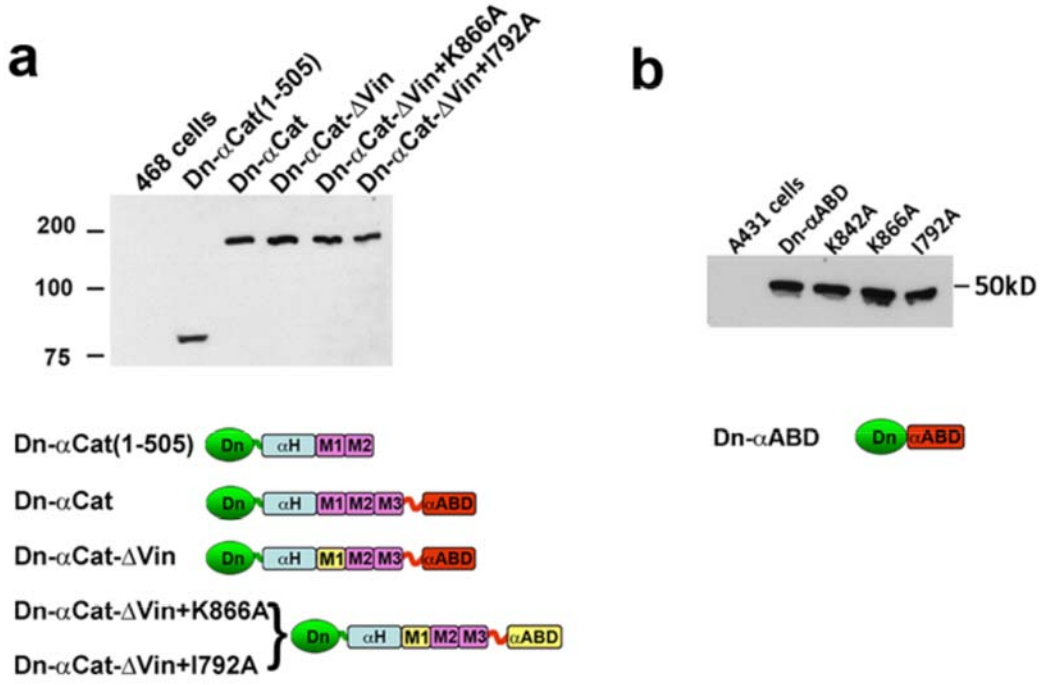

Figure S4. (**a**) Western blotting assays using the anti-α-Catenin antibody (EP1993Y) to probe expression levels of Dn-αCat and its mutants. Note that the parental 468 cells do not express endogenous α-catenin. (**b**) Anti-Dendra Western blot assays of A431 cells probing levels of expression of Dn-αABD and its point alanine mutants – K842A, K866A, and I792A.

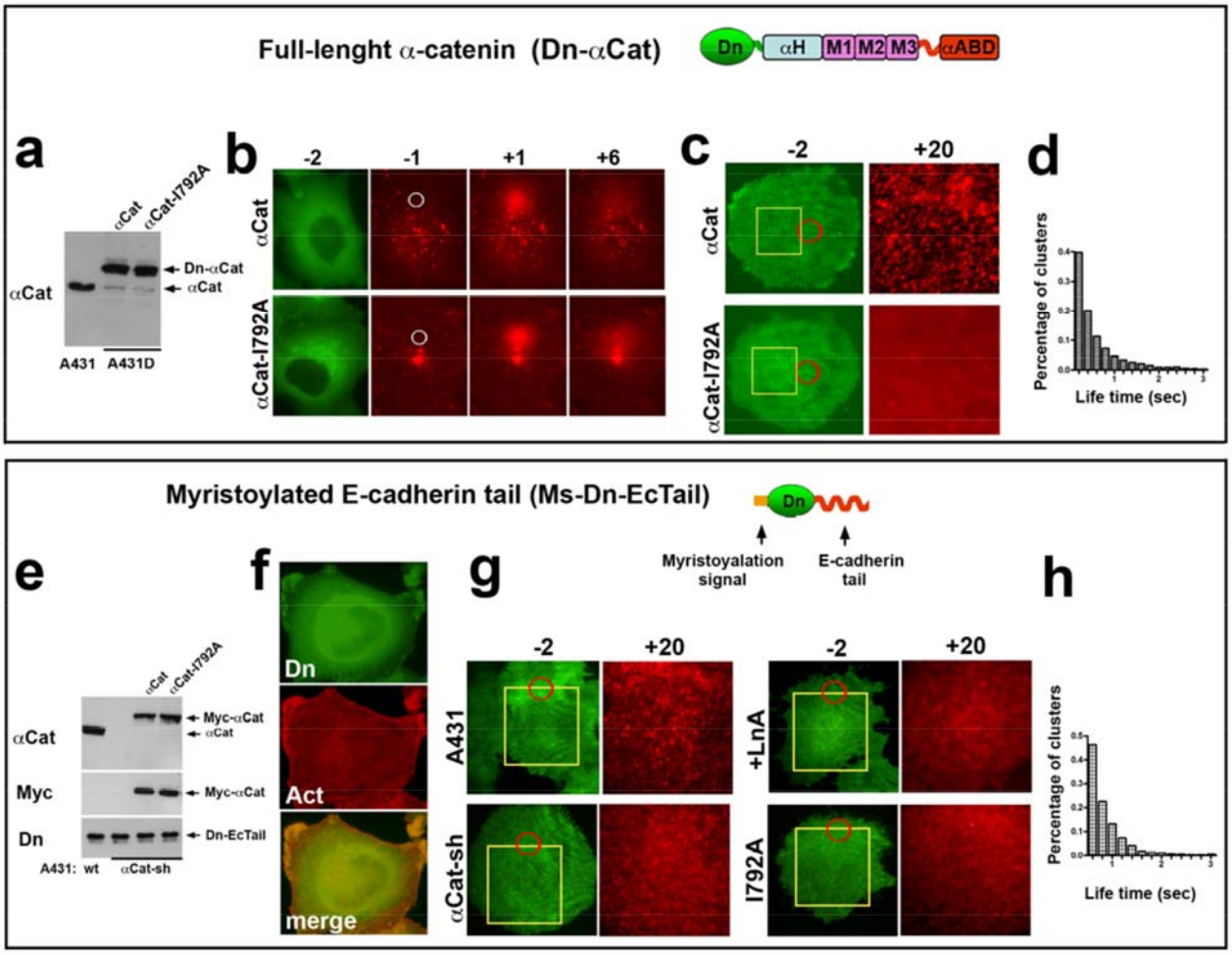

Figure S5. Dynamic properties of clusters formed by the full-length α-catenin (upper panel) and myristoylated E-cadherin tail (bottom panel).

Upper panel: Schematic representation of Dendra-tagged full length α-catenin (**a**) Wild type A431 cells (A431) and A431D cells expressing Dn-αCat (αCat) or Dn-αCat-I792A mutant (αCat-I792A) were analyzed by Western blot assay using anti-α-catenin antibody (αCat). Arrows indicate Dn-αCat (Dn-αCat) and the endogenous α-catenin (αCat). Note that the expression level of Dendra-tagged forms of α-catenin is similar to that of the endogenous α-catenin in A431 cells. Also note that cadherin-deficient A431D cells express very low endogenous level of α-catenin. (**b**) Dendra photoconversion assay of A431D cells expressing Dn-αCat (αABD) or its I792A mutant (αCat-I792A). See Fig. 9a for details. Only two frames taken one and six seconds after photoconversion (+1, +6) are shown. (**c**) Fluorescent speckle microscopy of A431 cells expressing Dn-αCat (αCat) or its I792A point mutant. See Fig 9c for details. (**d**) Lifetime distribution of α-catenin speckles.

Bottom panel: Myristoylated E-cadherin tail protein (Ms-Dn-EcTail) consisted of the myristoylation signal (yellow), Dendra2 (green), and E-cadherin tail, residues 771-882 (red) (**e**) A431 cells (wt), α-catenin-depleted A431 cells (αCat-sh), and the latter cells reconstituted either with the intact myc-tagged α-catenin (αCat) or with its I792A mutant (I792A) were stably transfected to express Ms-Dn-EcTail. Transgenes were probed using anti-α-catenin (αCat), anti-myc (Myc), and anti-Dendra (Dn) antibodies. Note that shRNA nearly completely depleted the endogenous α-catenin. (**f**) A431 cells expressing Ms-Dn-EcTail were stained for Dendra (Dn,

green) and actin (act). Note that the cell lamellas are enriched with both actin filaments and Ms-Dn-EcTail. (**g**) Fluorescent speckle microscopy of Ms-Dn-EcTail-expressing A431 cells (A431); the same cells after addition of Latrunculin A (+LtA); α-catenin depleted A431 cells (αCat-sh); and Myc-αCat-I792A-reconstituted α-catenin-depleted cells (I792A). (h) Lifetime distribution of Ms-Dn-EcTail speckles.